VĚDECKÉ SPISY VYSOKÉHO UČENÍ TECHNICKÉHO V BRNĚ

Edice Habilitační a inaugurační spisy, sv. 600
ISSN 1213-418X

Petr Neugebauer

HIGH FREQUENCY ELECTRON SPIN RESONANCE SPECTROSCOPY: TODAY AND TOMORROW

BRNO UNIVERSITY OF TECHNOLOGY
Faculty of Mechanical Engineering
Institute of Physical Engineering

Dr. Ing. Petr Neugebauer

HIGH FREQUENCY ELECTRON SPIN RESONANCE SPECTROSCOPY: TODAY AND TOMORROW

VYSOKOFREKVENČNÍ ELEKTRONOVÁ SPINOVÁ REZONANČNÍ SPEKTROSKOPIE: DNES A ZÍTRA

SHORT VERSION OF HABILITATION THESIS

FIELD: APPLIED PHYSICS

VYSOKÉ UČENÍ TECHNICKÉ V BRNĚ
NAKLADATELSTVÍ VUTIUM

BRNO 2018

KEYWORDS

Magnetic Resonance, Electron Spin Resonance (ESR/EPR), Single Molecule Magnets (SMMs), Dynamic Nuclear Polarization (DNP), High Magnetic Fields, THz frequencies

KLÍČOVÁ SLOVA

Magnetická resonance, elctron spinová resonance, jedno molecularní magnety, dynamická nukleová polarizace, silné magneticke pole, Terahertzové frekvence

MÍSTO ULOŽENÍ PRÁCE:

Habilitační práce je uložena v Areálové knihovně FSI VUT v Brně.

ISBN 978-80-214-5650-1
ISSN 1213-418X

TABLE OF CONTENTS

AUTHOR

Dr. Ing. Petr Neugebauer was born on September the 13th 1980 in Uherské Hradiště, Czech Republic. He was very active boy with lot of time spent in surrounding nature of his home town Kunovice, where he built up his passion for engineering and natural science in general. In 1996, he entered high school dedicated to mechanical engineering at Uherské Hradiště, followed by the engineering studies at Brno University of Technology (BUT), Czech Republic, at the Institute of Physical Engineering. In 2005, he finished his university studies by a diploma work dedicated to design of facility for in situ area monitoring of thin films (UV-VIS Reflectometry) under supervision of Prof. J. Spousta. During the university studies, he also spent six-months (Erasmus program) at Université Joseph Fourier, Grenoble & Institute Néel CNRS, Grenoble, France. Under supervision of Dr. L. Ranno, he was working on experimental research project dedicated to design and building of a high temperature - high impedance Hall effect measurement facility.

In 2005, he started his Ph.D. studies (Marie Curie fellowship through QuEMolNa FP6-CT-2003-504880 and Early stage researcher fellowship through MAGMANet FP6-NMP3-CT-2005-515767) in direction of magnetic resonance. His Ph.D. in Grenoble High Magnetic Field Laboratory under the supervision of Dr. Anne-Laure Barra dealt with the construction of high-frequency continuous wave and pulsed ESR (HFESR) spectrometers operating at 285 GHz. In the PhD project, he was fully responsible for the construction of the HFESR spectrometer. He developed a Fabry-Pérot resonator and a rotating sample holder for high magnetic field ESR applications based on piezoelectric steppers. This new concept, which led to significant improvement in sensitivity and crystal orientation precision, was adapted by other researchers in the ESR community. He successfully applied these methods to the study of the electronic properties of graphene and graphite (3x PRL) and single molecule nanomagnets, which led to 6 papers in high impact journals. He was the first who observed decoupled graphene by ESR spectroscopy, and could prove the extraordinary properties of graphene expressed by highest electron mobility ever reported in literature yet.

After finishing his PhD studies, he worked for two years as postdoctoral researcher (Stipendium: Center of Excellence Frankfurt - CEF) in the group of Prof. Thomas F. Prisner at the Goethe University and Biomolecular Magnetic Resonance Center (BMRZ) in Frankfurt, where his research was focused on combining HFESR and NMR spectroscopy, specifically concerning hyperpolarization of nuclei (Dynamic Nuclear Polarization, DNP) through the polarization transfer from electron to nucleus in order to enhance NMR signals. In this domain his work contributed to the development of the hardware as well as to the experimental method. He developed a unique method to determine saturation factor for the first time. His experiments led to the achievement of extremely large enhancements of the NMR signal of solvent molecules, leading to the reduction of the experimental time by three orders of magnitude, from hours to seconds.

Subsequently, he joined the group of Prof. Joris van Slageren in Stuttgart in 2012, where he was working on development and application of HFESR and Frequency Domain Magnetic Resonance (FDMR) at frequencies from 80 GHz to 1100 GHz and magnetic fields up to 17 T. His experience led to building of the worldwide state of the art and first modern HFESR/FDMR spectrometer at the University of Stuttgart in a very short time after arriving. It is the first spectrometer which can be operated either in the field domain (HFESR) by sweeping the magnetic field at fixed irradiation frequency, or in the frequency domain (FDMR), by sweeping the frequency at fixed magnetic

field. This very versatile and very sensitive spectrometer (10^7 spins/(Gauss.$Hz^{1/2}$)) and sets current worldwide state of the art. He used the spectrometer to solve many scientific questions which led, among the others, to more than 15 high impact papers, including papers in Nature Commun., Nature Phys. and J. Am. Chem. Soc. It attracts already attention of many scientists across the world, namely: Manchester (*UK*), Washington (*USA*), Bordeaux, Grenoble (*France*), Lisbon (*Portugal*), Valencia, Barcelona (*Spain*), Berlin, Leipzig, Stuttgart (*Germany*), Buenos Aires (*Argentina*), Brno, Olomouc (*Czech*), Vienna (*Austria*), Beijing, Xi'an (*China*), Dublin (*Ireland*), Copenhagen (*Denmark*).

In 2014, he received a DFG grant (NE1900/2-1, 240 kEUR) to study a THz and sub-THz excitations in graphene based materials by applying magneto-optical spectroscopy, through which he established his own research group. Later on, he was awarded by a DFG grant (SPP1601, NE1900/3-2, 250 kEUR) and Baden-Württemberg Elite Program stipend to further explore THz and subTHz spectroscopy at the University of Stuttgart.

In 2016, he received the ERC Starting grant "THz Frequency Rapid Scan – Electron Spin Resonance spectroscopy for spin dynamics investigations of bulk and surface materials (THz-FRaScan-ESR)", starting date 1.1.2018. The aim of the project is to set up and develop a revolutionary broadband THz Rapid Frequency Scan Electron Spin Resonance (THz-FRaScan-ESR) spectrometer, which will substantially increase the sensitivity of current magnetic resonance methods and, more importantly, it will allow multi-frequency relaxation studies even at zero field. This completely novel concept based on rapid frequency sweeps will stimulate development of novel materials and will improve MRI applications in hospitals.

In 2017, together with colleagues from institutions in Brno University of Technology, University of Stuttgart, Centro de Investigacion Cooperativa en Nanociencias CIC NANOGUNE and Thomas Keating Ltd. obtained European grant FET-Open supported by Horizon 2020 named "Plasmon Enhanced Terahertz Electron Paramagnetic Resonance (PETER)", starting date 1.1.2018.

He is author or co-author of 36 original scientific papers in ISI-indexed journals with over 1000 citations and h-index = 15 according to Web of Science, ResID I-7844-2013. He is a member of International EPR (ESR) society, German Priority Program (SPP1601) dealing with magnetic resonance spectroscopy and Elite program of Baden-Württemberg.

Since his Ph.D. studies Petr Neugebauer took a part in education of new students at different level of their carrier, including pupils. He is strongly determined to pursue a career in academia. He enjoys working with students. He was/is involved in teaching at the Institute of Physical and Theoretical Chemistry, Goethe University in Frankfurt am Main as well as at the Institute of Physical Chemisty, University of Stuttgart supervising Bachelor, Master and Ph.D. Students. Among the home universities, he is regularly lecturing at BUT, Czech Republic. He is regularly taking care of ERASMUS students from the BUT, supervising and mentoring their 6 month research stay at the Institute of Physical Chemistry, University of Stuttgart. Furthermore, in 2016, he was giving invited lectures (16 hours) at Beijing University and Xi'an University in China dealing with magnetic resonance spectroscopy. He supervised 2 PhD, 5 master and 6 ERASMUS students. Today, his research group is composed by 1 senior scientist, 3 postdoctoral researchers, 5 PhD and 2 MSc students.

From 1.1.2018, he became a group leader of Magneto-Optical & THz Spectroscopy (MOTeS) group at Central European Institute of Technology (CEITEC) in Brno University of Technology.

1 INTRODUCTION

High Frequency Electron Spin Resonance (HFESR) is a magneto-optical method where microwaves (MW) typically at frequencies of 100s of GHz (meV range), are used for exciting systems with unpaired electrons. HFESR is a powerful tool to investigate samples ranging from biomolecules to heterogeneous catalysts. It delivers the high g-value resolution that is needed to characterize the electronic structure and permits study of molecules in which magnetic anisotropy (zero-field splitting, ZFS) prevents investigations at lower frequencies. In materials science, it is also applied for measurements of modern solid state materials such as graphene (Chapter 3). In studies of coupled metallic centers with large ZFS (called molecular nanomagnets (MNMs) or single-molecule magnets (SMMs)), HFESR is an essential tool providing detailed information about their magnetic properties (Chapter 4). Furthermore, in the recent boom of Nuclear Magnetic Resonance (NMR) hyperpolarization, HFESR has had an indisputable role in improving NMR signal enhancement (Chapter 5). Historically, even small progresses in magnetic resonance have dramatically changed the landscape of what is possible in NMR, including MRI in hospitals. This has already led to 10 Nobel prizes in magnetic resonance.[1]

This works serves as a short introduction to the HFESR methodology and it is applications described in attached papers.

2 HIGH FIELD / HIGH FREQUENCY ELECTRON SPIN RESONANCE (HFESR)

This chapter will introduce Electron Paramagnetic Resonance (EPR), also called Electron Spin Resonance (ESR) or Electron Magnetic Resonance (EMR), which has become a major tool in diverse fields ranging from biology and chemistry to solid state physics and materials science. We start from the first realization of this experimental technique by E. K. Zavoisky and continue towards to more sophisticated techniques used nowadays. The basic principles of magnetic resonance as well as the advantages of going to higher magnetic fields and higher excitation frequencies (HFESR) will be discussed.

2.1 HISTORICAL OVERVIEW

The EPR technique was first invented by E. K. Zavoisky at the end of the Second World War in

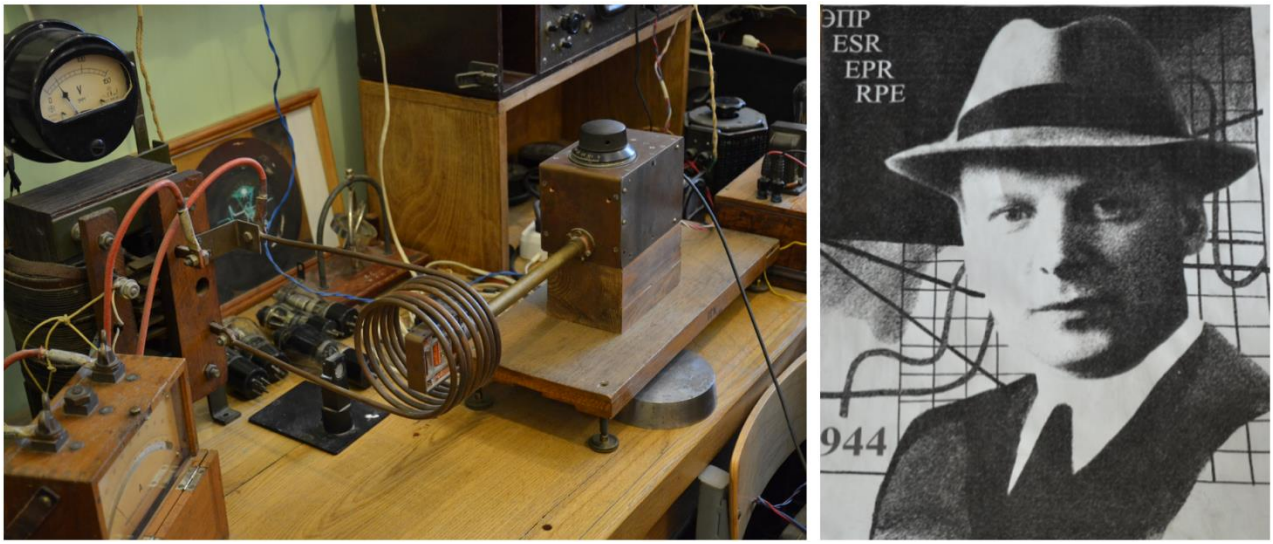

Figure 1. First ESR spectrometer operating at 10 MHz and 7.5 Oe designed by E. K. Zavoisky (1907-1976) in 1944 in Kazan. Pictures kindly provided by S. Zvyagin.

Kazan (USSR, today Russia) as a consequence of the availability of microwave (MW) components developed for RADAR. He employed the newly developed MW techniques in the construction of the first ESR spectrometer (Figure 1).[2] Soon after him, two years later (in 1946) in United States, and independently of E. K. Zavoisky, the Nuclear Magnetic Resonance (NMR) technique was developed by E. M. Purcell together with his colleagues R. Pound and H. Torrey at Radiation Laboratory at Massachusetts Institute of Technology.[3] E. M. Purcell together with F. Bloch (Stanford University) were honored in 1952 by the Nobel prize: "for their development of new methods for nuclear magnetic precision measurements and discoveries in connection therewith".[1] The work of E. K. Zavoisky was recognized much later on and he was honored posthumously by the prestigious ISMAR Award of the International Society of Magnetic Resonance in 1977.

First experiments, NMR and ESR, were performed in the continuous wave (cw) regime. In 1950, E. L. Hahn conducted an experiment at University of Illinois with radio frequency (rf) pulses and observed a nuclear spin echo, which was the starting point not only for pulsed NMR techniques.[4] However, in ESR it took a decade until first coherent manipulations of electronic spin were done in sodium-ammonia solutions[5], on electron donors in silicon[6] and the first pulsed ESR spectrometers were developed and described.[7] At the same time the pulsed NMR experiment already start to fully explore the possibilities of pulsed techniques. This was the point when NMR and ESR techniques continued in different ways. Whereas for NMR it was much easier to create coherent MHz pulses and thus fully explore the pulsed technique, creating new pulse sequences, multi-dimensional experiments etc., the situation for EPR was completely different. Today NMR almost completely moved from cw to pulsed operation, except for rare solid state physics applications. The problem in creating sufficiently short pulses and detecting fast transitions, often more than one order of magnitude faster than in NMR, limited ESR mainly to cw-ESR applications for a long time.

In 1957, G. Feher (*born in Bratislava, Czechoslovakia in 1924*) published his work in Bell labs where he pointed out the importance of the increase of the irradiation frequency for the sensitivity and the resolution of ESR spectrometers,[8] see Figure 2. However, it took a few decades until this prediction could be experimentally realized. The first to overcome the initial problems was the group of Ya. S. Lebedev from Moscow in the 1970s with the implementation of the first 148 GHz (D-band)/5.3 T ESR spectrometer.[9] The work of Lebedev was followed by several groups across the world in the 1980s. The group of W. R. Potter (Roswell Park Memorial Institute, Buffalo, New York) used 70 GHz (V-band)/ 2.5 T spectrometer to investigate trapped electrons in irradiated single crystals of polyhydroxy compounds.[10] The group of K. Möbius (Freie Universität Berlin) reported in 1984 an ESR spectrometer operating at 94 GHz (W-band)/3.4 T.[11] In 1988, the group of J. H. Freed (Cornell University) pushed the limit to 250 GHz/8.9 T by applying quasi-optics (QO) made of Teflon lenses in ESR for the first time.[12] The first pulsed HFESR spectrometer operating at 95 GHz was reported in 1989 by the group of J. Schmidt (Huygens Laboratory, Leiden).[13] Simultaneously, a multi-frequency high field ESR spectrometer was developed by L.-C. Brunel (Grenoble High Magnetic Field Laboratory, GHMFL) going to fields as high as 20 T using resistive magnets.[14, 15] In 1992, group of R. G. Griffin (Francis Bitter National Magnet Laboratory, Massachusetts Institute of Technology) reported pulsed spectrometer operating at 140 GHz.[16] At the same time in the Griffin group, the first pioneering work on high frequency Dynamic Nuclear Polarization (DNP) is conducted.[17, 18] Few years later, in 1995 a pulsed HFESR spectrometer operating even at 604 GHz using a pulsed far-infrared laser was reported in GHMFL. This renaissance was further boosted by reporting in 1998 an ESR spectrometer relying on QO techniques based on reflection (mirrors) and corrugated waveguides by the group of P. C. Riedi (St. Andrews University), with respect to transmission (lenses) used previously, this way low loss broadband HFESR spectrometers are used nowadays in most HFESR laboratories.

ESR methods are progressing now as fast as the NMR technique in the second half of the last century. X-band (10 GHz), Q-band (35 GHz), W-band (95 GHz) and even 263 GHz pulsed ESR

spectrometers are commercially available (mainly from Bruker or Jeol) and many pulsed experiments have become routine (ESEEM, HYSCORE, etc.). Double resonance techniques such as PELDOR[19] (DEER)[20] enable determination of the structure and kinetic properties of large molecules, which for different reasons were impossible before[21] and have become a useful complementary method to NMR and X-ray diffraction techniques in structure determination. Moreover, both techniques NMR and ESR are combined in DNP experiments, where ESR transitions are used to polarize nuclei via electron polarization transfer. The HFESR development is also strongly driven by the DNP experiments pioneered by Griffin at high fields and high frequencies.[17, 18] DNP experiments at ESR frequencies of 263 GHz, 329 GHz and 394 GHz corresponding to proton NMR frequencies of 400 MHz, 500 MHz and 600 MHz, respectively, are becoming routine equipment of NMR labs. Today many laboratories are still developing their own HFESR equipment[22-27], pushing the work on new methodology and application of ESR further.[28-32]

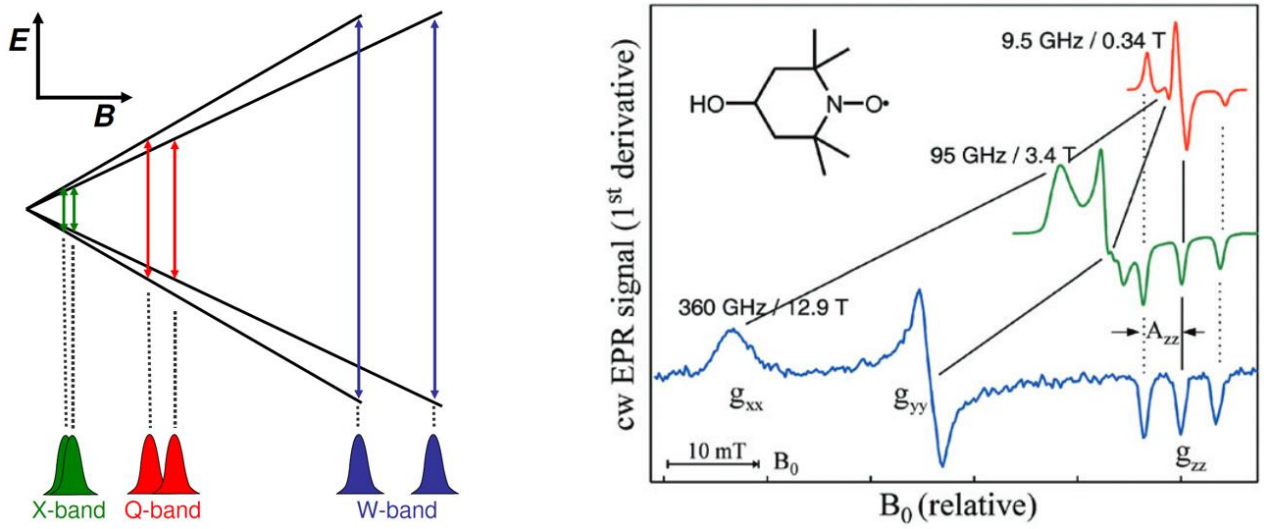

Figure 2. *Left*: Schematic visualisation of the effect of increasing magnetic field on the spectral resolution of two species with close g-values. Whereas at X-band (10 GHz) frequencies the species are overlapping at W-band (95 GHz) frequencies they are fully resolved. *Right*: First-derivative cw EPR spectra of a nitroxide radical (OH-TEMPO) in frozen water solution at different microwave frequency normalized to applied magnetic field B_0. The spectra are plotted relative to the fixed g_{zz} value. Note the increased resolution of the anisotropic g-factor, picture reprinted from reference.[33]

2.2 PRINCIPLE OF MAGNETIC RESONANCE

Particles such as, for instance, electrons or nuclei possess an intrinsic magnetic moment called spin, marked *S* or *I*, respectively. In case of electron, the total magnetic moment *J* of a particle is composed of its spin *S* and its orbital moment *L* ($J = L + S$). In presence of an external magnetic field **B**, the total magnetic moment starts to precess around the direction of the applied field **B** with an angular (Larmor) frequency $\omega_L = \gamma\mathbf{B}$, where γ is gyromagnetic ratio. The main difference between ESR and NMR techniques is in the magnitude of the Larmor frequency, which is connected to the gyromagnetic ratio $\gamma = qg/(2m)$, where *q* is charge, *g* is g-factor and *m* is the mass either of the electron or the nucleus which is about three orders of magnitude higher. The difference in mass of the electron with respect to the nucleus leads to resonances at different frequencies. When in ESR the resonance is observed in the GHz range, in NMR occurs at MHz frequencies. The lower frequency makes the experiment technically easier, thus the NMR technique progressed much faster than ESR.

ESR can be easily explained on the hydrogen atom which has one electron ($S = 1/2$, $L = 0$). In zero external magnetic field, the electron has two degenerate eigenstates, called spin UP ($M_S =$

+1/2) or spin DOWN (M_S = -1/2). The presence of an external magnetic field **B** removes the degeneracy of the ±1/2 spin states (Zeeman effect). The energy difference ΔE (Zeeman splitting) between the upper and lower state is

$$\Delta E = hf_{ex} = \mathbf{g}_e \mu_B \mathbf{B},$$

where $\mathbf{g}_e$ is the g-factor (Lande factor) of the electron and μ_B is the Bohr magneton. The above equation implies that the splitting is directly proportional to the external magnetic field **B**. Resonance absorption can occur if we apply an appropriate oscillating magnetic field $\mathbf{B}_1$, perpendicular to the external field **B**, oscillating at frequency f_{ex}. Similar resonance expression can be written to NMR. However in the real experiment, we do not manipulate/excite only one spin, but ensemble of many spins, which are in a sample. We introduce magnetization **M**, a macroscopic value describing sum of all spins in the sample, which is manipulated during the experiment. To describe the time evolution of **M** during the experiment semi-classically, Bloch equations are commonly used. More details about the description of the magnetic resonance experiment can be found in one of the recommended text books of J. A. Weil & J. R. Bolton[34] and J. Keeler.[35]

Furthermore, from the above expression it can be deduced that if there is a g-anisotropy, at higher fields, and thus at higher frequencies, it can be better resolved. This is schematically demonstrated on two species of slightly different g-values (Figure 2). Whereas at X-band frequencies and even at Q-band frequencies, it could be very difficult to resolve the two components correctly, at W-band frequencies they could be already completely separated and the g-values resolved correctly (Figure 2). The resolution of a W-band spectrometer can be considered as one order of magnitude higher than that of an X-band spectrometer; at 300 GHz the factor is about 30, if no broadening of the absorption lines is induced at higher frequencies. For the same reasons, HFESR leads to enhanced spectral resolution for powder patterns, originating from orientation distribution. For instance, this is the case of a sample containing only the radical TEMPO in a non-oriented form (powder or frozen solution, Figure 2*Right*). The $\mathbf{g}_e$ principal values as well as the hyperfine interaction associated with the z-axis (A_{ZZ}) are in HFESR clearly observed. The spectrum of the same sample at X-band (9.5 GHz) frequency collapses in a single line signal with hyperfine structure. It is much more complicated to obtain the g-anisotropy or to associate the field independent hyperfine interaction to the z-axis. Beside the increased resolution the HFESR allows access to paramagnetic species which possess large Zero Field Splittings (ZFSs) as it is in case of Single Molecule Magnets (Chapter 4). SMMs are difficult to study without HFESR. Beside above mentioned advantages, HFESR also provides higher sensitivity thanks to enhanced Boltzmann factor.

2.3 ESR SPECTROMETER

EPR spectroscopy has been the object of many technical changes and improvements within the last decades as was already mentioned. The improvements went hand in hand with developments in different fields of physics, e.g. physics of semiconductors (detectors and sources of MWs), physics of superconducting materials (magnets), astronomy (QO propagation) etc. Thanks to these developments, ESR spectrometers could move to higher frequencies and pulsed operation could also be implemented. The development of high frequency and HFESR spectrometers allowed resolving of many phenomena difficult or even impossible to observe before. Especially, it allowed determining of small *g* differences and accessing integer spin systems with large ZFSs (which were called “ESR silent" before). In this section, a general overview of the HFESR spectrometer operating in continuous wave (CW), pulsed mode or in frequency domain will be given.

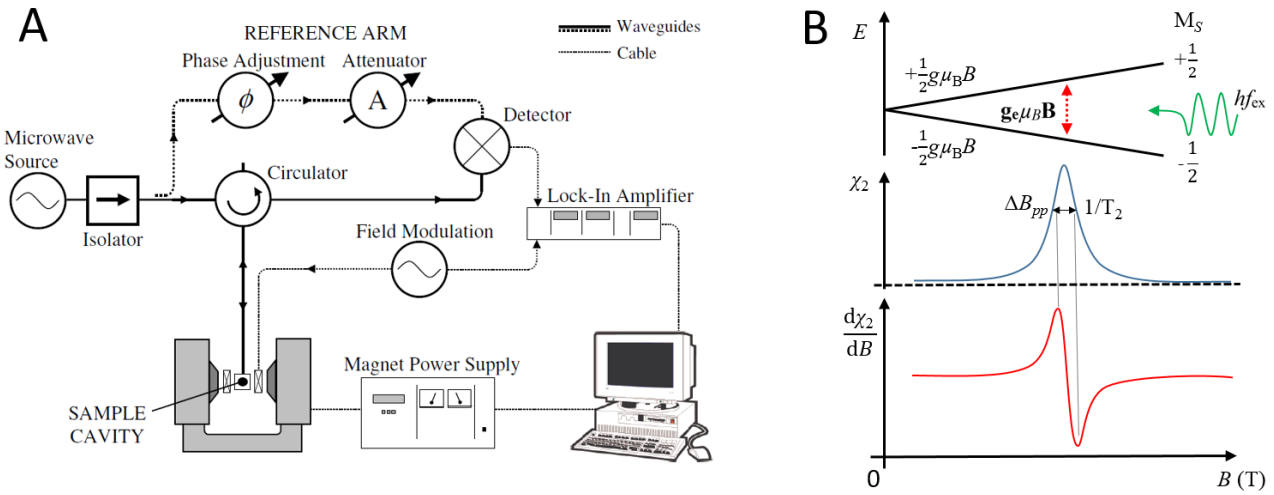

Figure 3. A) Schema of typical cw-ESR spectrometer operating in homodyne configuration with all its components indicated in the figure. B) An illustration of ESR experiment.

2.3.1 Cw- ESR

With respect to NMR, the ESR spectrometers operated in cw mode are still dominant in ESR community. This is due to that cw-ESR is simple and offer very valuable contain of information especially when it is performed at several frequencies - multi frequency ESR (Figure 2*Right*).

The cw-ESR spectrometer (Figure 3A) is composed of a stable MW source (typically Klystrons, Traveling Wave Tubes, Gunn diodes, High Frequency Amplifiers, IMPATT diodes etc.).[36] The MW is then directed from the source either by rectangular waveguides up to W-band frequency or through QO in HFESR spectrometers. MW goes through an isolator which protects the source from unwanted backward reflected MW. MW is directed to a sample, which is located in a MW resonator to enhance weak B_1 field on the sample, which is either single mode resonator at low frequencies or typically Fabry-Pérot resonator at high frequencies. The resonator is located in the center of magnetic field which is slowly changing and the ESR spectrum is recorded as a function of it at constant irradiation frequency (field domain). The magnetic field is either generated by resistive magnets (up to 3 T) or by superconducting coils. In addition to the main magnetic field B, a small modulation magnetic field is added, which oscillates at frequencies of several kHz in order to increase sensitivity by phase sensitive detection. At magnetic resonance, MW is absorbed (changed), as a result, Q-factor of the cavity is changed (drop of Q), which leads to increase of reflected MW from the cavity. The backward reflected MW goes towards a circulator, which directs the ESR signal into a detector (mixer, zero biased detector, bolometer etc.). The signal is decoded at the modulation frequency and the resulting ESR spectrum is then derivative of an absorption spectrum (Figure 3B).

2.3.2 Frequency Domain Magnetic Resonance

ESR has traditionally been performed at a fixed MW frequency (GHz range), while sweeping the external field (field domain). This was done for reasons of limited sweepability of MW sources used. In addition, working at a fixed frequency allows using a cavity or other type of resonator to enhance the sensitivity of the inherently insensitive ESR technique. In the 1960 and 70s, a number of Frequency Domain Magnetic Resoance (FDMR) studies had appeared mainly by Sievers and Richards.[37, 38] This work was essentially discontinued after 1980. From the late 1990s, the technique was revived by Mukhin, Dressel and Van Slageren,[39-42] and later also by Schnegg.[43] Only limited studies could be conducted due to available broadband sources. Nowadays, especially in the terahertz range, broadband sources are available. Working instead at fixed magnetic field and sweeping MW frequency (frequency domain) has distinct advantages. First of all, for many

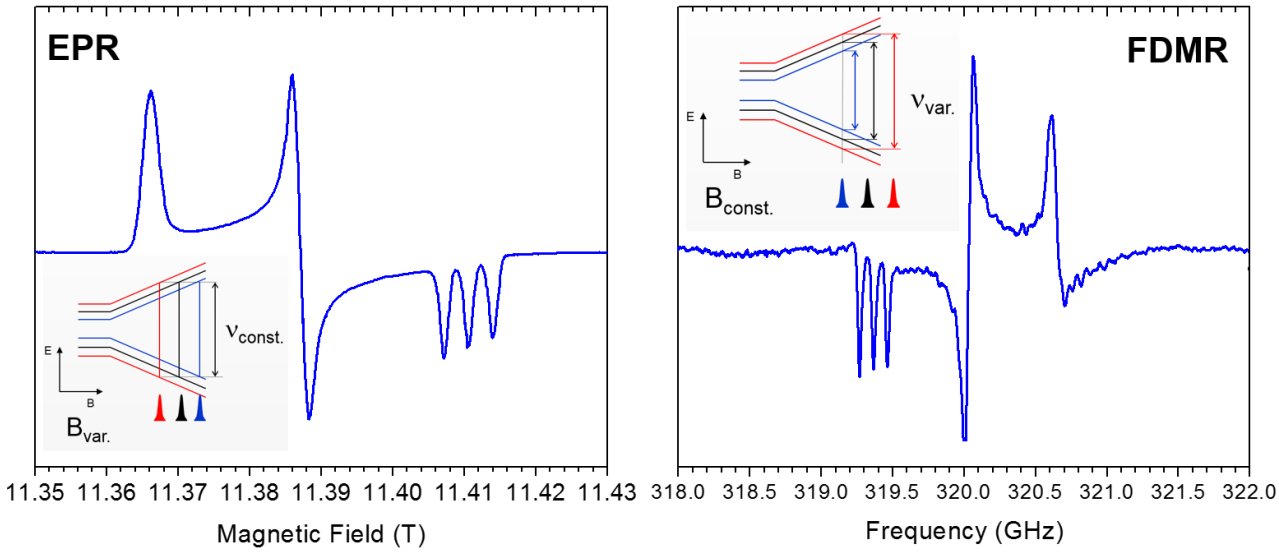

Figure 4.: Schematic explanation of ESR (EPR) and FDMR spectra. While in EPR, the MW frequency is kept constant and the spectrum is recorded as a function of magnetic field, in FDMR it is the opposite. This results in an "inverted" spectrum. In EPR, the first observed transition is that which corresponds to the highest g-value whereas in FDMR it is the last, as shown in the bottom part of the figure.

samples the energy splittings of interest are caused by field independent interactions, such as zero-field splitting or crystal field splitting (single molecule magnets). In a FDMR spectrum recorded even at zero field, the energy spectrum of the material under study is then directly read off. In contrast, in the field domain, the HFESR spectrum must be recorded at many different frequencies, where subsequent extrapolation to zero field gives the energy spectrum. Thus, FDMR is inherently faster than HFESR. Secondly, if the energy spectrum spans a very broad energy range up to several THz, the magnetic fields required for HFESR cannot be achieved with dc magnets any longer. Thirdly, FDMR spectra can be recorded while the superconducting magnet is in persistent mode, thus saving on the nonrenewable resource of liquid helium. Finally, applying a sizable magnetic field can change the properties of the sample itself, and can also lead to higher-order field dependent interactions becoming non-negligible. All these reasons favor performing experiments in the frequency domain.

The appearance of ESR and FDMR spectra can be seen on Figure 4, where ESR and FDMR spectrum of ^{14}N-TEMPOL is shown. While in ESR, the MW frequency is kept constant and the spectrum is recorded as a function of magnetic field, in FDMR it is the opposite. This results in an "inverted" spectrum. In ESR, the first observed transition is the one which corresponds to the highest g-value whereas in FDMR it is the last, as shown in the insets of the figure. The drawback of the FDMR method is that it is very sensitive to any standing waves in the system, which can be seen in the FDMR spectrum (Figure 4*Right*).

2.3.3 Pulsed ESR

Since 1950, when first coherent pulsed manipulation of spins was observed by E. L. Hahn, many scientists dreamt about their own pulsed ESR spectrometer. Pulsed ESR experiments[44] were primarily used to determine spin relaxation times, T_1 – spin-lattice and T_2 – spin-spin relaxation (Figure 5.). Nowadays, since discovery of site-directed spin labeling[45, 46] by W. L. Hubble in 1989 at University of California one of the key application of pulsed ESR spectrometers is Pulsed Electron-Electron Double Resonance[19] (PELDOR or DEER[20]) spectroscopy, a method used to measure distance between typically two individual spins.[32, 47]

In the basic experiments shown in Figure 5 two pulses are used: π/2 (90°) and π (180°). The nomenclature comes from the angular change of the direction of magnetization **M** (ensemble of

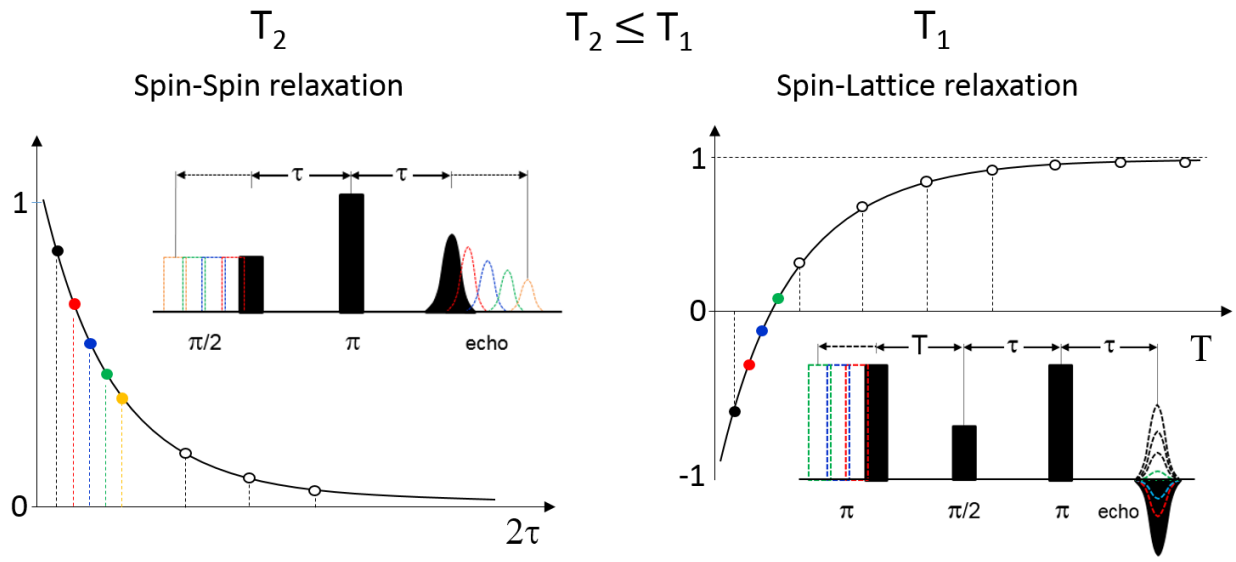

Figure 5. Two types of pulse experiments (sequences) used to determine T_1 (spin-lattice) and T_2 (spin-spin) relaxation times by pulsed ESR.

spins) which is manipulated during the experiment on a Bloch sphere and the time dependence of the magnetization is described by Bloch equations.[44] The first experiment in Figure 5 is used for determination of spin-spin relaxation time T_2 with the help of the *Hahn sequence* (π/2 - τ - π - τ - echo). The spacing τ between the pulses is changed step by step and the echo intensity I (proportional to M) is monitored. As the τ is rising the echo intensity decrease:

$$M(2\tau) = M(0).\exp(-2\tau/T_2)$$

The second type of experiment in the Figure 5 is called *inversion recovery* and it is used to determine spin-lattice relaxation time – T_1. In this experiment before the Hahn echo sequence is placed additional π pulse (π - T - π/2 - τ - π - τ - echo) separated by time T. During the experiment the Hahn echo sequence remain constant and the spacing T of the first pulse (π) is changing. The exponential curve is then recorded as a function of spacing T with respect to intensity of echo.

$$M_z(T) = M_z(0).(1 - \exp(-T/T_1)$$

The inversion recovery experiment can be understood as 180° rotation of a magnetized sample in the applied magnetic field and the further observation of how the magnetization tends to align with magnetic field. The equilibrium magnetization $M_z(0)$ is inverted opposite to the magnetic field by π pulse and its recovery is monitored by the Hahn echo sequence.

Pulsed ESR instruments with respect to cw-ESR experiment are demanding on a MW source. In order to access fast relaxation times the pulses should be short therefore, the MW source has to provide very high B_1-field on the sample. Typically π/2 pulses of length of few nanoseconds and MW sources of several hundreds of Watts are used.

3 SOLID STATE MATERIALS – GRAPHENE

Graphene is a relatively young material, observed for the first time in 2004 by K. S. Novoselov and A. K. Geim.[48] Since its discovery, graphene has fascinated thousands of scientists as well as engineers around the world. Today there is more than 120 000 publications dealing with graphene according to Web of Science. Graphene, which is the basic unit for the construction of bulk

graphite,[49] consists of a one-atom thick two-dimensional (2D) lattice of carbon atoms with a honeycomb structure and has extraordinary electronic properties. The electronic properties are the consequence of its linear band structure (dispersion) in the vicinity of the K and K' points, often called Dirac points (Figure 6). At the Dirac points, the conduction and valence bands are touching each other, which makes graphene a zero gap semiconductor (or a zero-overlap semimetal). The linearity of the dispersion makes graphene unique with respect to conventional materials with a classical parabolic dispersion, leading to charge carriers (electrons and holes) acting as massless particles, Dirac fermions, with a Fermi velocity v_F of about 10^6 m·s^{-1} which approaches the speed of light. These unique properties of graphene do not only exist at very low temperatures and extreme conditions, as might be expected, but they are preserved up to room temperature, as we and others have shown.[50] Combined, this makes graphene an excellent playground for probing quantum electrodynamic properties like the Klein paradox and Zitterbewegung and makes graphene a promising material for future applications.[51-55]

Recently, there has been a great deal of progress in preparation of manmade graphene by methods including chemical vapor deposition and epitaxial growth. However, the quality (in terms of electron mobilities) of these manmade graphene samples does not yet reach those of graphene decoupled from bulk graphite, evidenced by our observation of mobilities of 10^7 cm^2/(V·s) in graphene on graphite.[27, 56, 57] This extremely high mobility enables the Landau level quantization to appear at magnetic fields as low as 1 mT (see attached papers).[56] The ability to produce graphene of exceedingly high quality on a large scale is an essential prerequisite for the development of graphene-based devices. High-quality graphene displays ballistic electron transport at large distances which, if this material is successfully incorporated into devices, will lead to a breakthrough in electronics. It can be foreseen that in near future, graphene's superior material characteristics, ranging from its crystal structure over mechanical strength to the electronic properties will be elaborated in novel devices which are nowadays impossible due to limited quality of currently used materials.

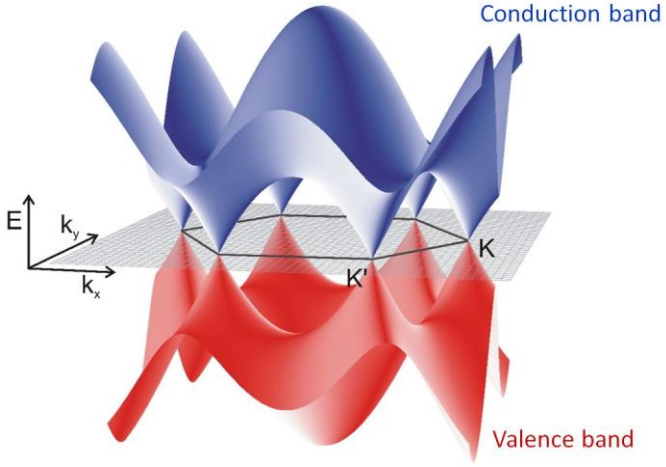

Figure 6.: Band structure (Brillouin zone) of graphene. The conductance (blue) and valence (red) bands touch at K and K' (Dirac) points in momentum space, around which the dispersion is linear, creating so-called Dirac cones.

3.1 CYCLOTRON RESONANCE

The electronic properties of graphene samples are typically investigated by transport measurements. However, these measurements only probe the Fermi level. Furthermore the transport measurement itself may cause defect formation in graphene, obscuring the properties intrinsic to the sample.[57] Spectroscopic measurements, on the other hand, allow noninvasive measurement of the electronic structure, not only in the vicinity of the Fermi level, but throughout the entire band structure. For the investigation of low-energy excitations, magneto-optical methods such as HFESR and far infrared (FIR) magneto-spectroscopy are relevant in particular, benefiting from their high sensitivities, as shown by a number of previous studies, including our own

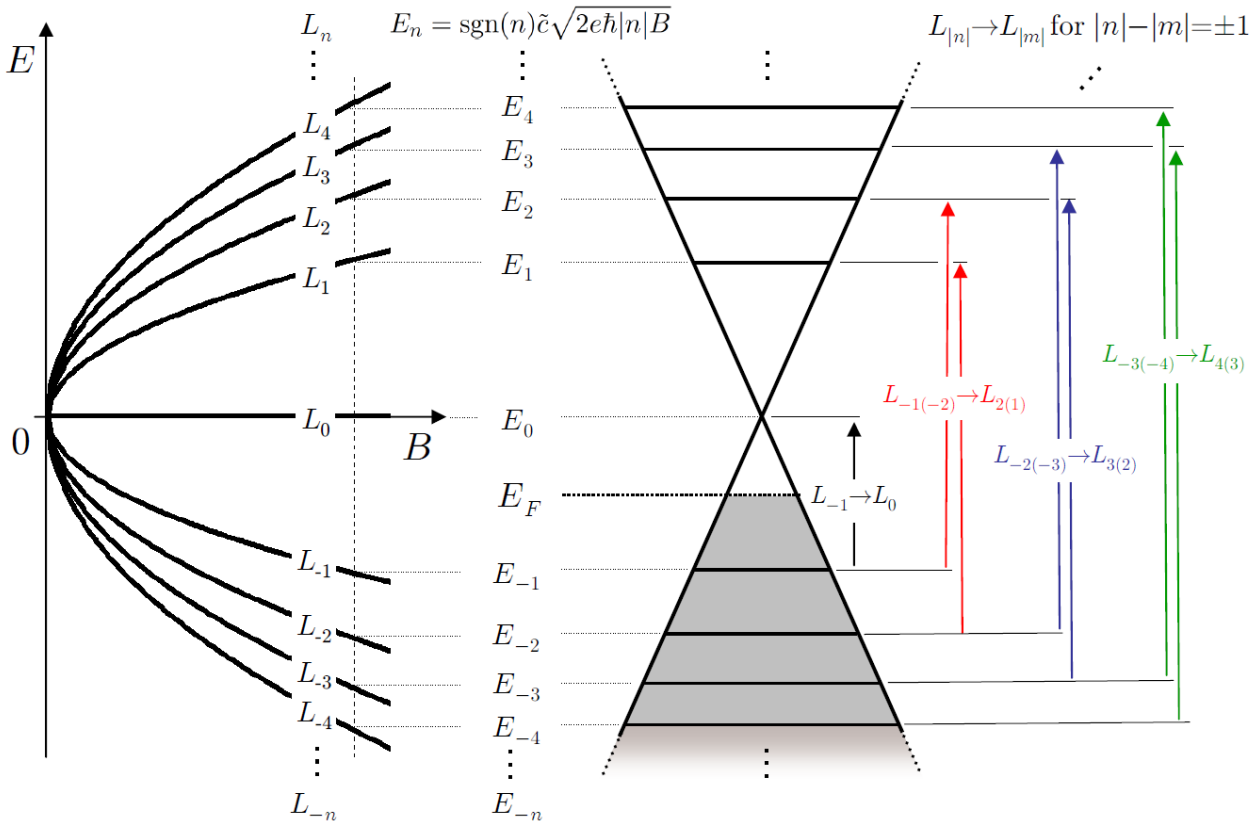

Figure 7.: Left: Schematic evolution of LLs L_n in graphene with applied magnetic field **B**. Right: Optically allowed transitions in *p*-doped graphene for a given magnetic field **B**. n and m denote indexes of LLs.

works.[50, 56, 58] Of these methods, HFEPR probes the lowest energy range between 100-1000 GHz (0.4-4 meV), while FIR typically probes the energy range from 1 to 10 THz (4-40 meV). In magnetic field, the electronic states in graphene become quantized into Landau levels (LLs) E_n:

$$E_n = \pm v_F\sqrt{2e\hbar B|n|}\,, \qquad n = \cdots, -2, -1, 0, 1, 2, \ldots$$

where n is the LL index, ± refers to electrons (+) and holes (-) states and e is the electron charge. Due to graphene's unique linear band structure, the LLs are not equally spaced and evolve with $\sqrt{B}$ (Figure 7). This implies rather high sensitivity of electronic states (LLs) in graphene to the applied magnetic field. Conversely, the investigation of the LLs in a magnetic field allows detailed understanding of the low-energy electronic structure of graphene.

On Figure 8, one can see how powerful HFESR is today with respect to previously used instruments. The Figure 8.A show experiments performed on single flakes of natural graphite of size 1 mm x 0.5 mm and thickness 25 µm recorded by the author in Stuttgart at 370 GHz and 5 K, unpublished. The spectrum is very rich. In the low field region signal originating from graphene is visible.[56] At fields of 0.05 – 0.80 T, about 20 cyclotron resonance harmonics are observed originating from conduction electrons in bulk graphite, where the fundamental cyclotron resonance can be observed at about 0.8 T. Signals at fields above 0.8 T are not fully understood and are currently under investigation. To compare the superior quality expressed by many spectral features of the present HFESR data, the averaged magneto-absorption spectrum of high quality graphite of diameter 1 cm and thickness 25 µm recorded by Galt *et al.* at 24 GHz and 1.1 K is shown in Figure 8.B.[55] In Figure 8C, the averaged magneto-absorption spectrum of pyrolytic graphite of size 1 cm x 0.7 cm and thickness about 1 mm recorded by Doezema *et al.* at 890 GHz and 4.2 K is presented.[59] Furthermore, the HFESR is very sensitive to impurities of investigated samples. This

is very valuable information to the industry dealing with the large scale production of graphene for future applications.

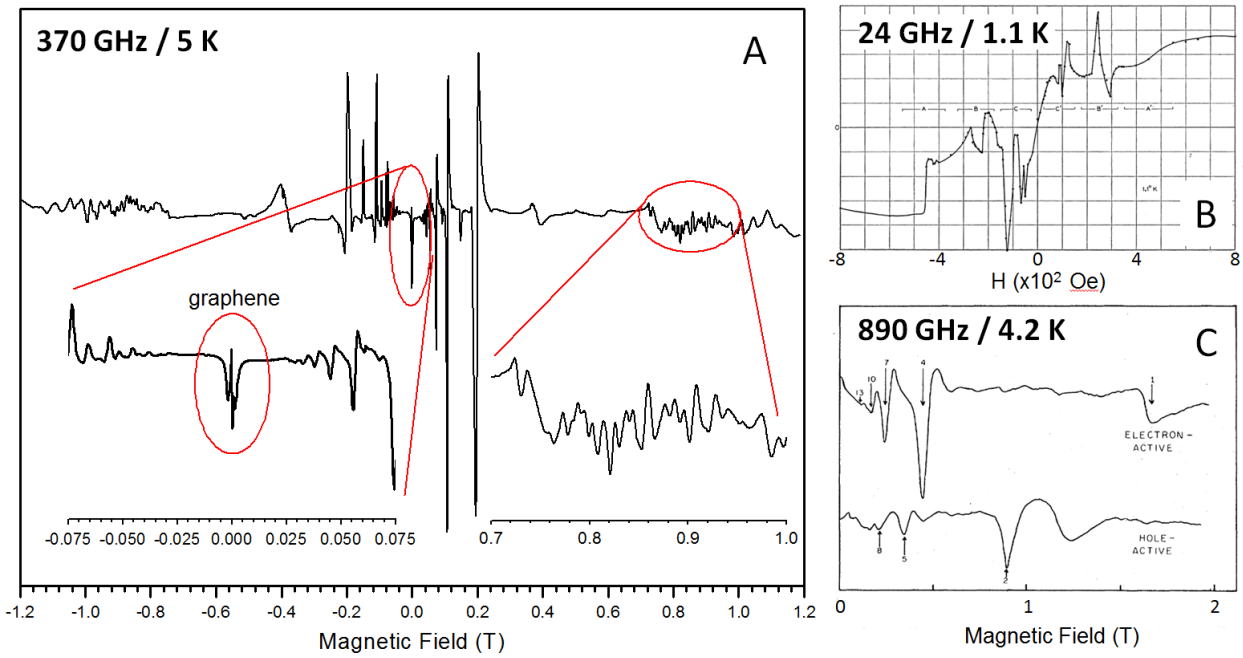

Figure 8.: A) A single shot magneto-absorption (HFESR) spectrum of natural graphite of size 1 mm x 0.5 mm and thickness 25 µm recorded by the author in Stuttgart at 370 GHz and 5 K, unpublished. The spectrum is very rich, where in the low field region signal originating from graphene (see attached papers) is visible, at fields above 0.8 T not fully understood spectral features are observed. For data quality comparison: B) An averaged magneto-absorption spectrum of high quality graphite of diameter 1 cm and thickness 25 µm recorded by Galt *et al.* at 24 GHz and 1.1 K, Ref. [54]. C) An averaged magneto-absorption spectrum of pyrolytic graphite of size 1 cm x 0.7 cm and thickness about 1 mm recorded by Doezema *et al.* at 890 GHz and 4.2 K, Ref. [58].

4 SINGLE MOLECULE MAGNETS

By the end of the 1980s, molecular magnetism had seen the emergence of a new research area: the study of high nuclearity spin clusters, which are complex molecules containing a large number of spins most often carried by transition metal ions.[60] Among these molecules, the ones possessing a large spin ground state associated with an Ising type anisotropy (Figure 9.A) have been under particular focus.[61] The macroscopic large spin of these molecular systems (Figure 9.B) together with a negative Zero-Field Splitting (ZFS) results in the presence of a barrier for the reversal of their magnetization at low temperatures. The main consequence is a slow relaxation which, below a blocking temperature, leads to a behaviour quite similar to the one of superparamagnets.[62] Due to these properties, they have been named Single Molecule Magnets (SMMs). At the low temperatures, they exhibit a hysteresis in their magnetization curve with a step-like shape (Figure 9.C), a signature of the presence of Quantum Tunneling of the Magnetisation (QTM).[63, 64]

HFESR proved to be one of the most powerful methods to precisely determine the magnetic anisotropy of SMMs. This chapter will introduce the power of HFESR spectroscopy in molecular magnetism on an example of a Fe_4-complex.[65]

4.1 INTRODUCTION TO SINGLE MOLECULE MAGNETS

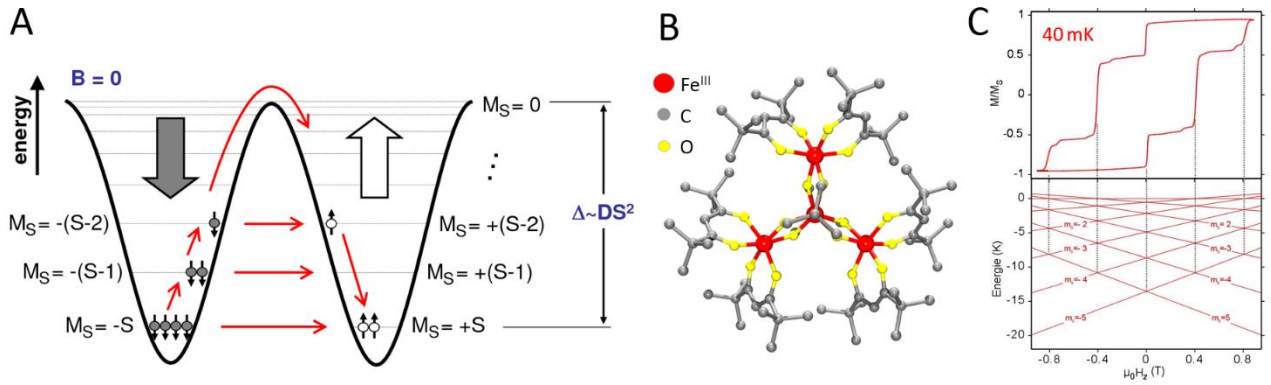

Figure 9.: A) Schematic description of energy levels in SMMs using double well potential (Ising type anisotropy) at zero magnetic field. The high of the barrier Δ between the two ground M_S states is proportional to the size of *D* (axial ZFS parameter) and S^2. Thanks to the energy barrier *Δ* the system can be blocked in one of the M_S state. The system relax into equilibrium either overcoming the energy barrier or via Quantum Tunneling of Magnetization (QTM). B) Fe_4 complex is an example of SMM which is composed by four antiferomagneticaly coupled Fe^{III} ions with spin of 5/2 leading to a total giant spin of molecule 5. C) A hysteresis loop recorded for the Fe_4 complex at 40 mK. Typical steps in magnetization are observed due to QTM presented in SMMs between the opposite M_S states on the other side of an energy barrier.

SMMs possess a large spin ground state *S*, resulting from exchange interactions between their magnetic centers. Often, it is possible to stabilize a large spin ground state even when only antiferromagnetic interactions are present, due to the competition between all the magnetic exchange pathways resulting from the structure of the molecule. As SMMs have an easy-axis magnetisation, their spin ground state *S* is resulting in a negative axial ZFS term, *D*. Thus, inside the ground multiplet, the levels $M_S = \pm S$ are the lowest in energy and the level $M_S = 0$ is the highest, the energy difference being $\Delta \approx DS^2$ for integer *S* and $\Delta \approx D(S^2\text{-}1/4)$ for non-integer *S*, where Δ is an energy barrier for the reversal of the magnetization (Figure 9A). At temperatures, when only the ground spin state is thermally populated, the relaxation time of the magnetization increases due to the presence of spin reversal barrier *Δ* and it is dependent on types of the active relaxation processes. In the high temperature region these processes originate in relaxation of magnetization to the lattice phonon bath through the lattice vibrations, phonons. The relaxation processes can be distinguished to three basic types: Orbach process (two phonon relaxation process allows spin to reorient by climbing over *Δ*, fundamental for occurrence of SMMs), direct process (a single-phonon process involving the phonons with the same energy as the magnetic resonance quantum *hν*, spin relaxation without a need to overcome *Δ*), Raman process (two-phonon process with strong temperature but no magnetic field dependence).[66] At the lowest temperatures relaxation will take place through quantum tunnelling of the lowest M_S states and will be temperature independent. The step-like shape of the magnetic hysteresis curve is the signature of a relaxation involving QTM. The steps in the magnetisation curve (Figure 9C) appear when tunnelling is made possible by energy levels degeneracy. If Δ is sufficiently high (and relaxation processes other than Orbach are suppressed) the magnetisation can be preserved for a long time. Therefore, it is in principle possible to store information in such a molecule. The first complex identified to behave as a SMM was the $Mn_{12}Ac$ complex.[61, 67] Despite being the first SMM discovered and despite the enormous synthetic effort to increase *Δ*, the $Mn_{12}Ac$ complex lost the record of the highest temperature for which magnetic hysteresis was observed two decades after its discovery and new record was set by unique Mn_6 complex.[68, 69] However, due to difficulties of obtaining SMMs with large energy barrier using polynuclear transition metal

complexes[70, 71] the interest moved to mononuclear SMMs so called Single Ion Magnets (SIMs) based on lanthanides and actinides. The great interest is due to their large angular momenta and their huge anisotropies.[72] The origin of the huge magnetic anisotropy is a consequence of the crystal field (CF) splitting of the ground multiplet of the lanthanide ion.[73] These properties engender slow relaxation of the magnetic moment to SMM behavior, making them potentially suitable for use in novel ultrahigh-density magnetic data storage devices in future. The strategy proved to be successful and recently, SIM with high blocking temperature and even magnetic hysteresis at 60 K was reported for organometallic Dy(III) compound.[74]

Besides the interest in increase of Δ, another important trend in SMM research nowadays is examining SMM behavior of the complexes organized on solid surfaces or anchored to them.[75-77] For applications such as information storage, quantum computing[78-80] or molecular spintronics[81, 82] it is necessary to find a way how to deposit molecules on suitable substrates and maintaining their properties when deposited on the surface. In the following text, the power of HFESR utilization is described on an example of Fe_4 SMMs, which retained their SMM properties even after they were grafted on a surface.[76]

4.2 HFESR AND SMMS

HFESR proved to be one of the most powerful methods to precisely determine the magnetic anisotropy of SMMs.[65, 83-105] In this section, we highlight some of the most important features of HFESR for the study of SMMs on a particular case of tetrairon(III) molecule. Due to the large anisotropy of SMMs, these complexes are inaccessible to classical ESR spectrometers operating at low frequencies (X-band, 0.3 cm^{-1}), either being ESR silent or giving rise to very incomplete spectra. Going to higher frequencies to overcome the energy gaps of the ground spin multiplet is necessary, also because SMMs have integer spin values. To give an (extreme) example, the splitting between the lowest occupied states $M_S = \pm 10$ and $M_S = \pm 9$ in the $Mn_{12}Ac$ is about 10 cm^{-1} (300 GHz); hence ESR spectrometers operating at low frequencies cannot probe this transition.

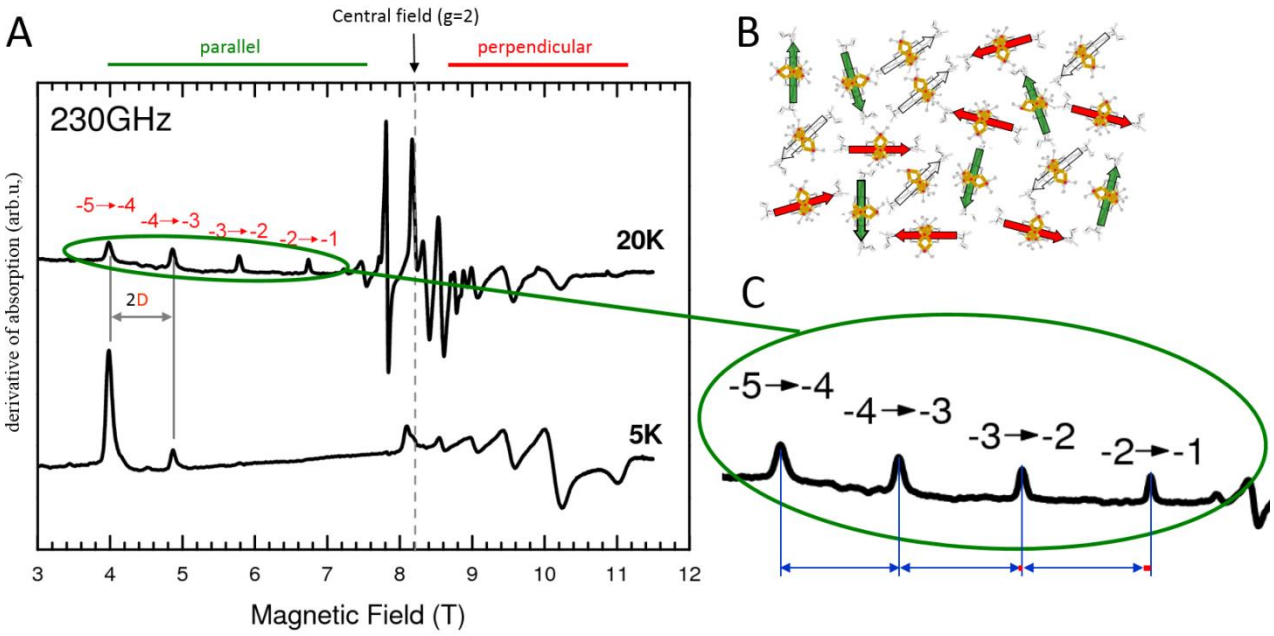

Figure 10.: A) HFESR spectrum of compressed powder of Fe_4 complex 2 from Ref. [64] recorded at 230 GHz, 5 and 20 K. B) schematic representation of a powdered sample with highlighted magnetic orientation of the molecules with respect to external magnetic field. C) Detailed view on $M_S \pm M_{S\pm1}$ transitions in parallel region indicating presence of higher order terms by increasing spacing between the consecutive transitions.

4.2.1 Spin Hamiltonian

To interpret the ESR spectra of SMMs the Giant Spin Hamiltonian formalism is used:

$$H = H_Z + H_{CF} = \mu_B \mathbf{S}\cdot\mathbf{g_e}\cdot\mathbf{B} + D[\mathbf{S_z}^2 - \tfrac{1}{3}S(S+1)] + E(\mathbf{S_x}^2 - \mathbf{S_y}^2) + \sum_{k,q} B_k^q O_k^q$$

where $\mu_B \mathbf{S}\cdot\mathbf{g_e}\cdot\mathbf{B}$ is the Zeeman Hamiltonian H_Z associated with the external magnetic field **B**, and $D[\mathbf{S_z}^2 - \frac{1}{3}S(S+1)] + E(\mathbf{S_x}^2 - \mathbf{S_y}^2)$ is the crystal (ligand) field Hamiltonian which describes the magnetic anisotropy (ZFS) of the system at second order. S_x, $\mathbf{S_y}$, $\mathbf{S_z}$ are the three components of the spin operator **S**. The *D* and *E* terms are the axial and rhombic anisotropy parameters of the system. They are related by $-1/3 \leq E/D \leq +1/3$. When the ratio $E/D = 1/3$ the system is totally rhombic, whereas in the case of E = 0 the system is axially symmetric. *D* can be either negative or positive, corresponding to an easy-axis or an easy-plane anisotropy respectively. The last term in the spin Hamiltonian $\sum_{k,q} B_k^q O_k^q$ describes higher order terms associated with a large spin values S, where O_k^q are Stevens operators and the B_k^q are the corresponding parameters, which are defined by the symmetry of the complex.[106]

4.2.2 Powdered Samples

HFESR spectra of SMMs are usually easy to analyze**.** The ZFS parameters can be obtained from HFESR either on polycrystalline (powdered) or single crystal samples. The powdered samples are pressed into pellets (in our case typically 20-30 mg of a sample is used for 5 mm pellet) in order to avoid orientation effects caused by strong magnetic field. Powder HFESR spectrum is often recorded only, because sufficiently large amount of information on magnetic anisotropy can be extracted from its analysis.

Powder spectrum contains information about all possible orientations of the investigated sample. The powdered samples are pressed into pellets (in our case typically 20-30 mg of a sample is used for 5 mm pellet) in order to avoid orientation effects caused by strong magnetic field. On the Figure 10, experimental powder spectra obtained for a Fe_4 sample (complex 2 in Ref.[65]) at 230 GHz, 5 K and 20 K are shown. When we look on the HFESR spectrum, we can divide the

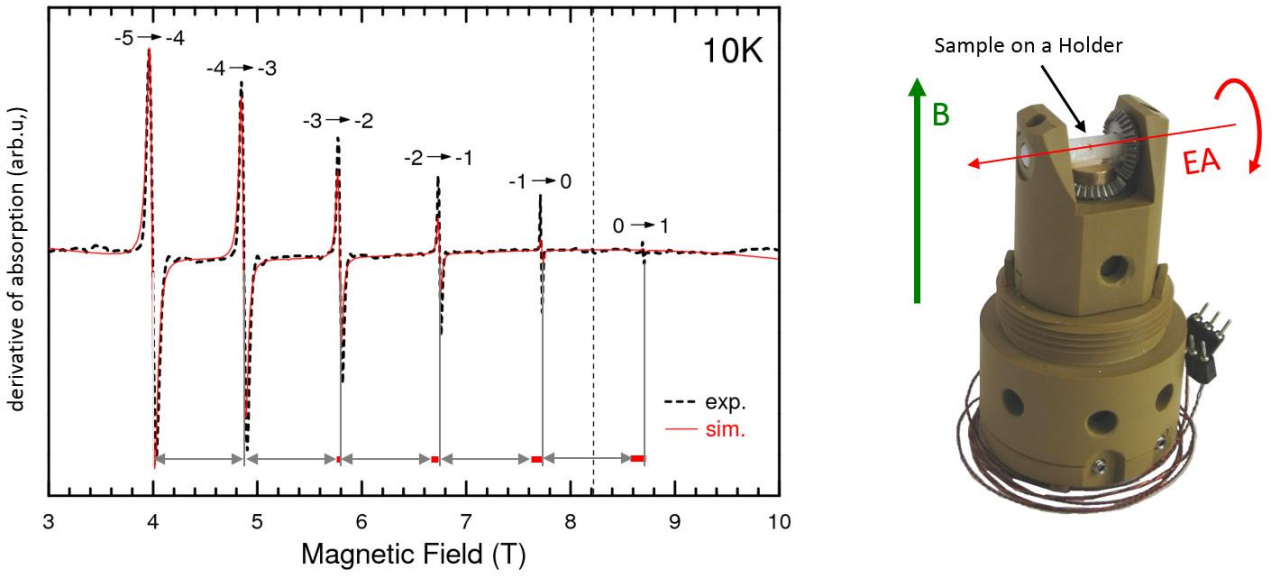

Figure 11.: Single crystal HFESR spectrum of the same Fe_4 complex as in Figure 10 recorded at 230 GHz and 10 K in orientation of magnetic field applied along easy axis of the Fe_4 complex. Right: Photograph of developed a single crystal rotator used in our single crystal studies with the rotation around easy-axis (EA) perpendicular to applied magnetic field, rotation in hard plane, see Ref. [81].

spectrum into two parts, perpendicular and parallel around the central g-value (8.2 T). From the size of these two regions, we can determine the sign of *D* parameter of ZFS. In this particular case the sign is negative. The parallel region corresponds to signal coming from molecules with easy-axis aligned with the applied field. Conversely, the signal in the high field part of the spectrum corresponds to the magnetic field in the hard-plane. The negative sign of the *D*-parameter is further confirmed by the measurements at elevated temperature, where we see rise and decrease of the peak amplitudes in the parallel region, note the peak at 4 T. Furthermore, the $M_S \pm M_{S\pm1}$ transitions can be easily assigned and the spacing between the consecutive peaks is proportional to $2D$, $D = -0.449$ cm^{-1}. The careful inspection of the spacing of the parallel transitions (Figure 10C) reveals that the line-to-line separation slightly increases when moving to high magnetic field, thus pointing to presence of higher order terms of Giant Spin Hamiltonian, which are better distinguished from a single crystal measurements.

4.2.3 Single Crystal Studies

Single crystal studies are performed in order to obtain a better knowledge of the magnetic anisotropies, especially to determine magnitude of the higher order terms in the Giant Spin description. Figure 11 shows a single crystal HFESR spectrum of the same complex as in Figure 10 recorded at 230 GHz and 10 K with the orientation of the easy-axis along applied magnetic field **B**. From complete single crystal studies (Figure 12), recording of spectra along the easy-axis and the complete rotation in the hard plane (rotation around C3 axis, easy axis of Fe_4 complex) allows precise determination of the higher order terms.[86]

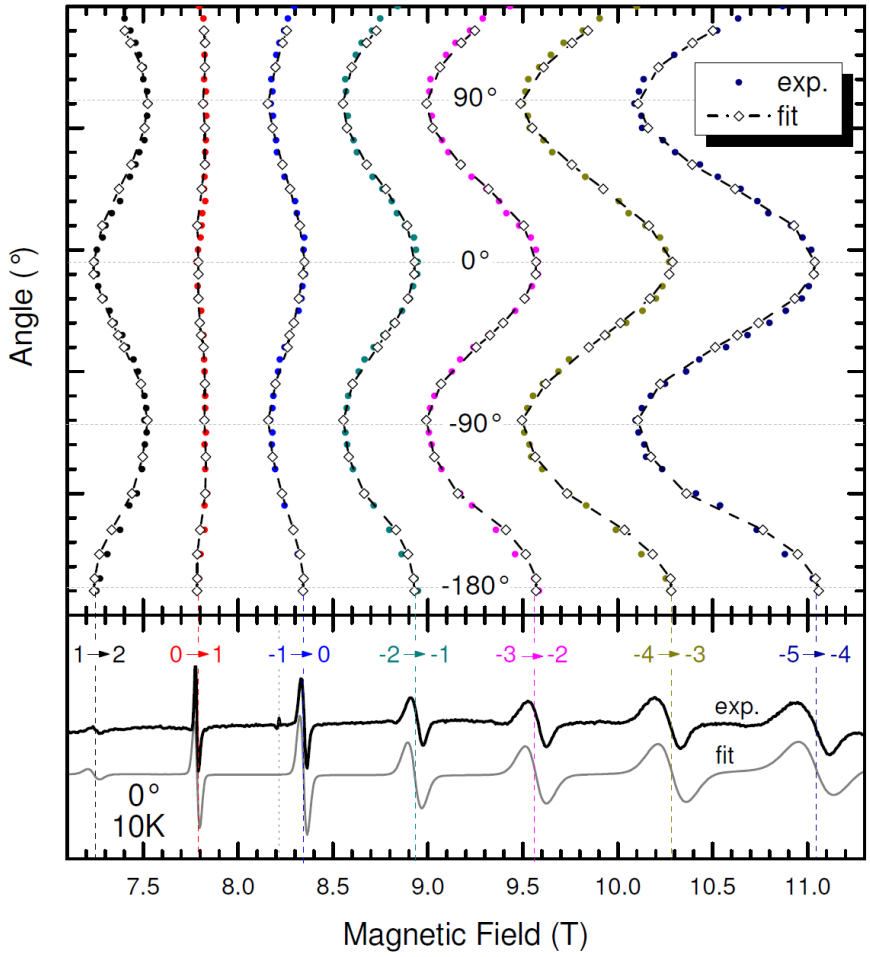

Figure 12.: Map of evolution of resonance lines of Fe_4-complex in the rotation around easy axis, with applied field in hard plane, together with corresponding simulation.

5 DYNAMIC NUCLEAR POLARIZATION (DNP)

Nuclear magnetic resonance (NMR) is an intrinsically insensitive technique, with Boltzmann distributions of nuclear spin states on the order of parts per million in conventional magnetic fields. On the other side electrons have typically three order of magnitude higher polarization with respect to nuclei. To overcome the low sensitivity of NMR caused by the low polarization, dynamic nuclear polarization (DNP) can be used to gain more than the three orders of magnitude in signal enhancement by a polarization transfer from electrons to nuclei. This enormous increase in NMR signal enhancement will lead in decrease of experimental time by six orders of magnitude. As already mentioned, historically, even small progresses in magnetic resonance spectroscopy have dramatically changed the landscape of what is possible in NMR, including MRI in hospitals. This has already led to 10 Nobel prizes in magnetic resonance.[1] In DNP experiments, nuclear spin polarization is enhanced by transferring the relatively larger electron polarization either from native paramagnetic center or by adding polarizing agents[107, 108] to NMR active nuclei by microwave irradiation of ESR transitions.[17, 18, 109-111]

A. W. Overhauser proposed the idea to polarize nuclei in metals by applying MW excitation to the electron resonance transition already in 1953 at University of Illinois,.[112] The experimental proof of this concept was shown by T.R. Carver, C.P. Slichter (from the same institute as A. W. Overhauser) on Li metal at low magnetic fields even before the theoretical paper was published.[113] The DNP work was mainly focused on examination of experiments at low frequencies and fields. The DNP renaissance started with the work associated mainly with Griffin group at MIT in early 1990, performing experiments at 5 T.[17, 18] The Griffin group was mainly focused on solid state DNP and have demonstrated polarization transfer mechanisms that scale more efficiently with applied field than previously expected.[114] DNP enhancements of –10 for ^{1}H and –40 for ^{13}C were observed on the solid sample using magic angle spinning (MAS) DNP on polystyrene doped by BDPA (α, γ–bisdiphenylene–β–phenylallyllyl) radical at room temperature and were considerably larger than expected.[17] MAS-DNP experiments on real life samples of arginine and the protein T4 lysozyme came soon after with observed enhancement over 100.[18] The liquid state DNP took another decade until J. H. Ardenkjær-Larsen perform his experiment in Malmö, Sweden in 2003.[115] The obtained enhancement over 10 000 in ^{13}C spectrum (natural abundance) of urea using a trityl radical and dissolution DNP triggered the rush in DNP spectroscopy. Today, MAS-DNP is routine experiment in many NMR laboratories and liquid state DNP is still undergoes certain development.[116]

5.1 LIQUID STATE DNP

Improving sensitivity is a key issue in NMR spectroscopy. Even a small signal enhancement by a factor of 2 shortens the acquisition time by a factor of 4. Now imagine, what it would be possible to track in NMR experiments if the experimental times on MRI machines in hospitals would be shortened by several order of magnitude. There is strong belief that this enormous increase in sensitivity and time will be possible by implementation of liquid DNP into hospital applications. In the liquid state, the active DNP mechanism is the Overhauser effect. The theoretical description of Overhauser DNP in liquids is based on the Solomon equation[117] with steady state solution for Overhauser enhancement ε_{OE}:

$$\varepsilon_{OE} = \frac{\langle I_z \rangle - I_0}{I_0} = -\frac{\gamma_e}{\gamma_n} \cdot f \cdot s \cdot \xi$$

where $\langle I_z \rangle$ is nuclear magnetization and I_0 is the nuclear polarization in thermal equilibrium. γ_e and γ_n are the gyromagnetic ratios of the electron and the nucleus, respectively, *i.e.* $\gamma_e/\gamma_n \approx -660$ for protons,[118] $f=1-T_{1R}/T_{1W}$ is the leakage factor, which can be determined from the nuclear T_1 in the presence (T_{1R}) and in the absence of radicals in the solution (T_{1W}), and reflects the influence of radicals on nuclear relaxation rate of the used solvent. The factor *s* denotes the saturation factor, which describes how well the electron transition is saturated by the MW irradiation. It ranges from 0 for no saturation, *i.e.* thermal population, to 1 for a fully saturated electron spin transition with equalized populations. The saturation factor *s* depends on:

$$s = \frac{1}{n} \frac{\gamma_S^2 B_{MW}^2 T_{1e} T_{2e}}{\left(1 + \gamma_S^2 B_{MW}^2 T_{1e} T_{2e}\right)}$$

where *n* is number of ESR lines, B_{MW} is MW field on the sample, T_{1e} and T_{2e} are relaxation times of electron. The last parameter is called the coupling factor ξ. While the optimization of *f* and *s* is rather a technical issue, the coupling factor ξ reflects the nature of the polarization transfer between the electron and nuclear spins and cannot be easily controlled. The coupling factor ξ describes the efficiency of the cross-relaxation processes and is given by:

$$\xi = \frac{w_2 - w_0}{w_0 + 2w_1 + w_2}$$

where w_2 is double quantum relaxation rate, w_0 is zero quantum relaxation rate, w_1 is nuclear spin relaxation rate and w_2 is double quantum relaxation rate (Figure 13). The coupling factor depends on the dynamics and the energetics of the electron–nuclear spin system. For pure dipolar coupling it is a positive quantity, which can take the maximum value of 0.5 at low magnetic field values and decreases with increasing magnetic field.

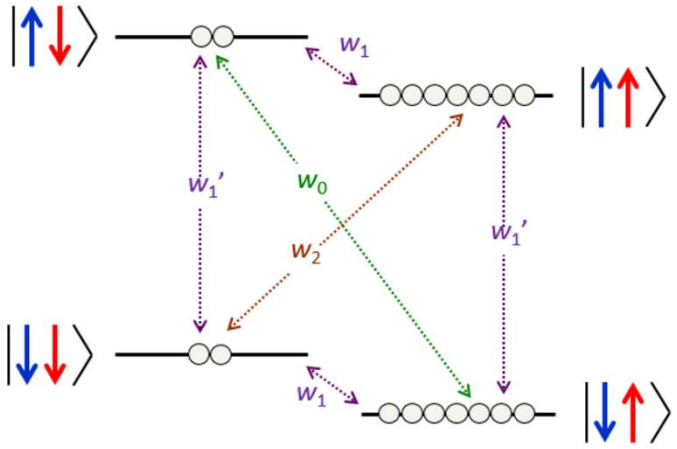

Figure 13.: Energy level diagram for an electron spin *S* = 1/2 (in blue) coupled to a nuclear spin *I* = 1/2 (in red). w_1: nuclear spin relaxation rate, w_1': electron spin relaxation rate, w_2: double quantum relaxation rate, w_0: zero quantum relaxation rate.

5.1.1 Experimental Techniques and Challanges

There are three types of approaches how to perform liquid state DNP spectroscopy at high magnetic fields. First is the original dissolution DNP, where sample is polarized at cryogenic

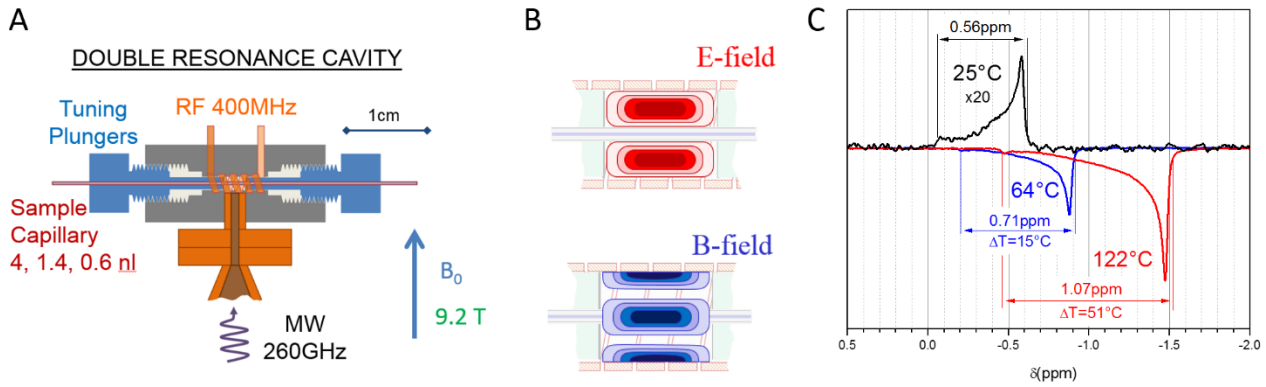

Figure 14.: A) Schema of a double resonance cavity for in-situ-DNP. The walls of cavity are made out of thin copper stripe and serves as a radio frequency (RF) coil as well as an outer walls for a TE_{011} MW cavity. The sample in a small capillary with outer diameter max. 150 µm is inserted through the plungers into the cavity, with sample volumes inside the active area indicated in the figure. The MW is coupled to the cavity from the bottom via small coupling hole in the copper stripe. B) Distribution of MW electrical and magnetic field inside the TE_{011} cavity. The sample heating is associated with the oscillating electrical field. C) ^{1}H-NMR signal obtained on water with 40 mM ^{14}N-TEMPOL radical in the double resonance cavity without applied MW (in black) and with MW (in color). Note, that the origin of the distorted ^{1}H-NMR peak is due to this particular experimental configuration. When the MW is applied the signal is inverted and the broadening of the original peak is visible, pointing out the temperature distribution over the sample.

temperature (bellow 5 K) and then hot liquid is injected in order to quickly warm up the sample.[115, 119] Second one is a shuttle-DNP, where the electron spins are excites at low magnetic fields and low frequencies, afterwards the sample or even the whole probe is shuttled rapidly into a high magnetic field for NMR detection.[120, 121] The third one is in-situ DNP, where MW excitation and detection is done at the same magnetic field.[109, 110, 122]

From the above is clear that the liquid state DNP is technically challenging and each approach has its advantages and disadvantages. In the first two approaches complicated devices have to be built in order to move or to dissolve the DNP sample, but the advantage of these approaches is that large samples (sample volumes) can be used. In the last case, the MW heating associated with high power MW irradiation has to be taken into account.

The in-situ-DNP was used by the author in investigation of DNP enhancement of water (paper 8) and organic solvents (paper 9). The schematic description of the experimental DNP double resonance cavity is shown on Figure 14.[122] The cavity was designed for 400 MHz ^{1}H-NMR and 263 GHz ESR. The walls of the cavity are made out of thin copper stripe and serves as a radio frequency (RF) coil with inner diameter of 1.48 mm as well as an outer walls for a TE_{011} MW cavity. The MW cavity is tuned using plungers with silver coating at the fronts. The sample is loaded in a capillary with outer diameter of 150 µm and with the inner diameters in the range from 10 µm to 100 µm. The capillary is then inserted through the plungers into the cavity. The sample volumes inside the active area of the cavity are indicated in the Figure 14A. The MW is coupled to the cavity from the bottom via small coupling hole in the copper stripe. As already mentioned, the key problem in in-situ-DNP is associated with MW heating, which is associated with the oscillating electrical field. The distribution of MW electrical field and magnetic field inside TE_{011} cavity is shown on Figure 14B. Even though, the electrical component of MW is well separated from the sample the MW heating can be enormous as can be seen from Figure 14C. The figure shows the ^{1}H-NMR signal obtained on water with 40 mM ^{14}N-TEMPOL radical without applied MW (in black) and with applied MW (in color). Note, the shape of the peak, which is in typical high resolution NMR about 1 Hz broad. The origin of the distorted peak is due to the fact that the tiny cylindrical sample is aligned perpendicular to applied field and the field is heavily distorted by the metallic structure of the cavity itself.[123] When the MW is applied the peak is inverted due to a negative enhancement. When we look closer on the broadening of the peaks one can estimate a

large temperature gradients over the tiny sample. The peak temperature can even well above boiling point (MW overheating).[109]

Up to now, DNP spectrometers were mainly based on high power continuous MW irradiation (tens of Watts) and the research was mainly focused rather on simple molecules than large biologically relevant molecules. These days, first experiments on larger molecules are performed and pulsed MW schemes become implemented, which may reduce MW heating.[124] Another challenges lie in optimization of polarizing agents (radicals) for liquid DNP experiments. Furthermore, there is still lot to do on the hardware side as well as on the DNP theory, as the observed experimental enhancements are still not fully understood.

6 CONCLUSIONS AND OUTLOOK

In this thesis I have introduced ESR technique as a powerful method in many directions of science. We started with historical development of the method to recent days. We introduce the principles of the conventional continuous wave (cw) ESR (field domain) with respect to Frequency Domain Magnetic Resonance (FDMR). The principles of pulsed ESR where shown on two basic experiments used to determine T_1 (longitudinal, spin-lattice) and T_2 (transversal, spin-spin) relaxations times. We then moved to the application of high frequency / high field ESR (HFESR) starting with applications in solid state physics, demonstrating the high sensitivity of recent instruments on graphene and graphite. Single Molecule Magnets (SMMs), where HFESR proved to be one of the most powerful methods to precisely determine the magnetic anisotropy of these systems, were introduced. The power of the technique was explained on an example of a Fe_4-complex. The last example in HFESR spectroscopy was its application in signal enhancement of NMR spectroscopy, Dynamic Nuclear Polarization (DNP). All that gave an overview of the application of HFESR up today.

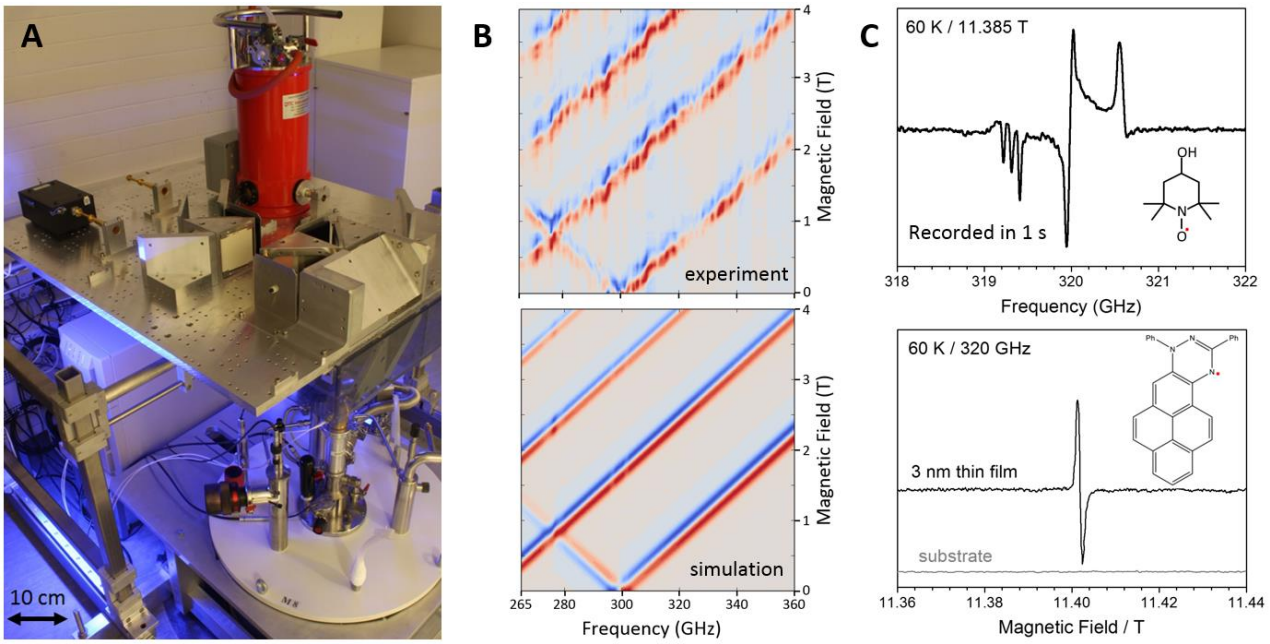

Figure 15.: A: The combined HFESR/FDMR spectrometer recently developed by me at the University of Stuttgart. B: First full field-frequency diagram of an oriented tiny crystal (0.1 mg) of the Mn12Ac single molecule magnet recorded only in 30 minutes with corresponding simulation below. C: Top: Single scan FDMR spectrum recorded in the non-resonant cavity in only 1 s for 1 mg of 100 µM of the 14N-TEMPOL radical (inset) at 60 K and magnetic field of 11.385 T. Bottom: Single scan HFESR of a thin layer (3 nm) of a Pyren-Blatter radical recorded at 60 K and at 320 GHz in the non-resonant cavity. The sample (inset) was prepared by Prof. Rajca, University of Nebraska–Lincoln, and the evaporation was carried out by PD Dr. Casu at the University of Tübingen. Note: All figures are unpublished results.

However much is still unknown about spin interactions with surfaces and spin dynamics at frequencies above 95 GHz. The standard method, pulsed HFESR, is not suitable for many crucial samples. Currently, the highest frequency commercially available pulsed HFESR spectrometer operates at a frequency of 263 GHz (at a cost of >1.5 M€). The spectrometer is restricted to that particular frequency and due to the use of cavities with mm dimensions only to either powdered or liquid samples. The pulsed 263 GHz ESR spectrometer uses very tiny single mode cavity of size 0.5 mm ($\lambda/2$) and the sample is placed into 100 μm capillary which limits all studies. It means that almost nothing is known about electron spin relaxation at higher frequencies, especially of thin films and bulk materials. This is particularly a problem in quantum computation at THz frequencies and the rapidly growing hyperpolarization methods in Nuclear Magnetic Resonance, where in both cases optimization of the spin relaxation of the system is essential. Furthermore, the combination of high MW power and the single mode cavity requires a delay (deadtime) between the end of the last excitation MW pulse and the start of data acquisition to allow the cavity response to ring down and to protect sensitive detectors from burn out. This means that pulsed ESR spectroscopy concept is inherently limited to relaxation times longer than several hundreds of nanoseconds. I recently set up the first broadband CW High-Frequency ESR/Frequency Domain Magnetic Resonance (HFESR/FDMR) spectrometer at the University of Stuttgart (Figure 15A), which operates seamlessly in a very broad frequency range from 85 GHz to 1100 GHz, and sets the current worldwide state of the art for broadband ESR spectrometers. It can be tuned to any frequency in the given range, for example to frequency specific to molecular motions. It is the first spectrometer which can operate either in the field domain (HFESR) by sweeping the magnetic field at fixed irradiation frequency, or in the frequency domain (FDMR), by sweeping the frequency at fixed magnetic field. The sample can be placed in a non-resonant cavity (5 mm in diameter), on a rotating sample holder (Figure 11*Right*) or in a tunable Fabry-Pérot resonator (Q = 1200 at 330 GHz). In FDMR, the spectrometer possesses a very high sensitivity, which led to the first FDMR measurement of a tiny single crystal of a SMM of mass only 0.1 mg (Figure 15B) as well as of a thin film with 100 μM 14N-TEMPOL radical embedded in 1 mg of polystyrene (Figure 15C Top). It is also possible to record spectra of only a 3 nm thin film of an organic radical (Figure 15C Bottom). This makes the HFESR/FDMR spectrometer an outstandingly

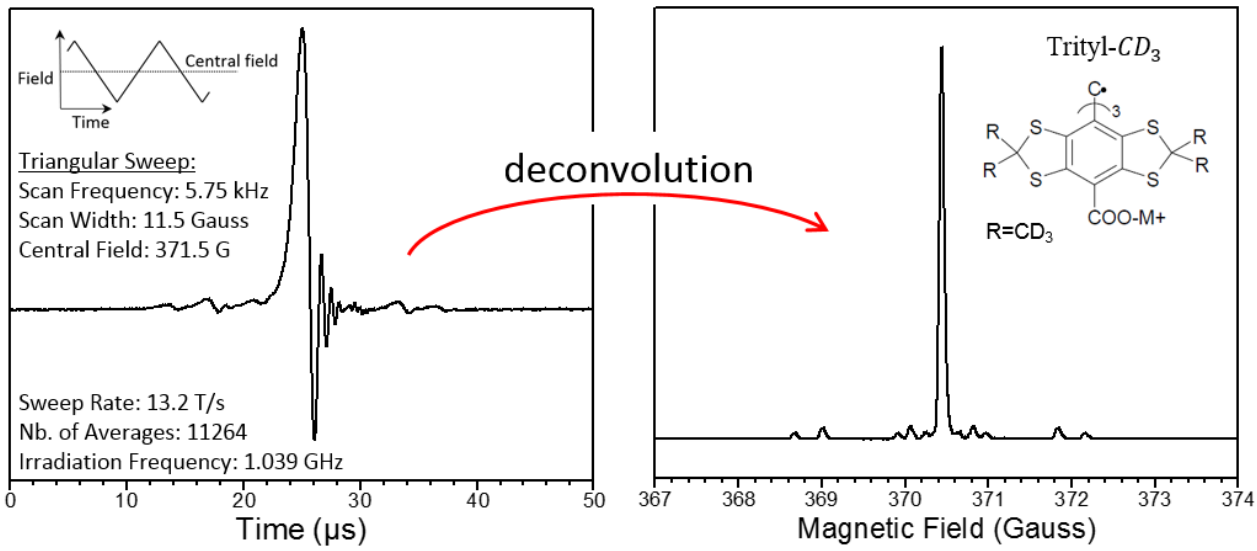

Figure 16.: Left: Rapid Field Scan ESR spectrum showing transient effects of 0.2 mM Nycomed triarylmethyl (trityl-CD3) radical recorded by author in the ESR centrum in Denver. The spectrum was recorded in 2 seconds using triangular magnetic sweeps with 11.5 G width and 5.75 kHz sweep frequency, corresponding to sweep rate of 13.2 T/s (~0.37 THz/s), at constant 371.5 G central field and irradiation frequency 1 GHz. Right: Deconvoluted rapid field scan ESR spectrum of the trityl-CD3 radical.

powerful tool. However, the presented HFESR/FDMR spectrometer is approaching its technical limits and it was not primary built for measurements of relaxation times.

The spin coherence time can be extracted from ESR, if the magnetic field sweep rate is fast compared to the relaxation times.[125] For sweep rates faster than the coherence time, the directly detected spectrum will show oscillations in the signal response (transient effects, wiggles) (Figure 16), which allow the determination of the coherence time.[126] Transient effects were first observed by Bloembergen in 1948 during his work in NMR spectroscopy.[127] This observation led to the development of correlation NMR and Fourier Transform (FT)-NMR spectroscopy by J. Dadok (*born in Dětmarovice, Czechoslovakia 1926*).[128, 129] In ESR, such effects were observed only much later.[130] Nowadays, rapid scan ESR, which was pioneered by the Denver group, is performed by few groups mainly at low frequencies (below 10 GHz) by fast magnetic sweeps at a constant microwave frequency using resonant cavities. This limits the experiments to narrow spectra (radicals), for which the spectral response fits within the bandwidth of the resonant cavity.[28, 29] However, the method can be reconsidered and instead of fast magnetic sweeps at constant frequency, fast frequency sweeps at a constant magnetic field can be implemented, similarly to FDMR (Figure 15B). Nowadays, it is possible by a current technology to build THz-Frequency-Rapid-Scan-ESR (THz-FRaScan-ESR) spectrometer capable of capturing spin dynamics of various systems at the user selected frequency in broad frequency range. The above described developments are already starting to be realized at Brno University of Technology, with the international team of PhD and MSc students under supervision of experienced scientists. With the strong belief, that we can put Brno back to the center of magnetic resonance development.[131]

7 ACNOWLEDGEMENT

It is very long list of people, which guided me to this point and to whom I would like to express my: THANK YOU! I would like to start with my parents, they were always supportive and passion over all the years. Teachers and tutors, who were very enthusiastic about the science and motivate me in the early years of my carrier. I would like to thank to my colleagues from Stuttgart and Frankfurt for creating nice environment and stimulating scientific atmosphere in the past years. Then, I would like to express my gratitude to Tomáš Šikola for kicking me out of "comfortable nest", Anne-Laure Barra and Wolfgang Wernsdorfer for the introduction to molecular magnetism and electron spin resonance spectroscopy. Milan Orlita, for nights spent by measurements of graphene. Last but not least to Thomas Prisner and Joris van Slageren for mentoring me on my way to scientific maturity, my life partner Lucie and our kids for all we are doing.

8 REFERENCES

1. C. Boesch, *J. Magn. Reson. Imag.*, 2004, **20**, 177-179.
2. E. K. Zavoisky, *Zh. Eksp. Teor. Fiz.*, 1945, **15**, 253.
3. E. M. Purcell, H. C. Torrey and R. V. Pound, *Phys. Rev.*, 1946, **69**, 37-38.
4. E. L. Hahn, *Phys. Rev.*, 1950, **80**, 580-594.
5. R. J. Blume, *Phys. Rev.*, 1958, **109**, 1867-1873.
6. J. P. Gordon and K. D. Bowers, *Phys. Rev. Lett.*, 1958, **1**, 368-370.
7. D. E. Kaplan, M. E. Browne and J. A. Cowen, *Rev. Sci. Instrum.*, 1961, **32**, 1182-1186.
8. G. Feher, *Bell Syst. Tech. J.*, 1957, **36**, 449-484.
9. M. A. Ondar, A. A. Dubinskii, O. Ya. Grinberg, J. A. Grigor'ev, L. B. Volodarskii and Y. S. Lebedev, *Zhurnal Strukturnoi Khimii*, 1981, **22**.

10. H. C. Box, E. E. Budzinski, H. G. Freund and W. R. Potter, *J. Chem. Phys.*, 1979, **70**, 1320-1325.
11. E. Haindl, K. Möbius and H. Oloff, *Z. Naturforsch.*, 1985, **40a**, 169-172.
12. W. B. Lynch, K. A. Earle and J. H. Freed, *Rev. Sci. Instrum.*, 1988, **59**, 1345-1351.
13. R. T. Weber, J. A. J. M. Disselhorst, L. J. Prevo, J. Schmidt and W. T. H. Wenckebach, *J. Magn. Reson.*, 1989, **81**, 129-144.
14. F. Muller, M. A. Hopkins, N. Coron, M. Grynberg, L. C. Brunel and G. Martinez, *Rev. Sci. Instrum.*, 1989, **60**, 3681-3684.
15. A. L. Barra, L. C. Brunel and J. B. Robert, *Chem. Phys. Lett.*, 1990, **165**, 107-109.
16. T. F. Prisner, S. Un and R. G. Griffin, *Israel Journal of Chemistry*, 1992, **32**, 357-363.
17. L. R. Becerra, G. J. Gerfen, R. J. Temkin, D. J. Singel and R. G. Griffin, *Phys. Rev. Lett.*, 1993, **71**, 3561-3564.
18. D. A. Hall, D. C. Maus, G. J. Gerfen, S. J. Inati, L. R. Becerra, F. W. Dahlquist and R. G. Griffin, *Science*, 1997, **276**, 930-932.
19. A. D. Milov, A. B. Ponomarev and Y. D. Tsvetkov, *Chem. Phys. Lett.*, 1984, **110**, 67-72.
20. G. Jeschke and Y. Polyhach, *Phys. Chem. Chem. Phys.*, 2007, **9**, 1895-1910.
21. M. Bennati and T. F. Prisner, *Reports on Progress in Physics*, 2005, **68**, 411.
22. M. Rohrer, O. Brügmann, B. Kinzer and T. F. Prisner, *Appl Magn Reson*, 2001, **21**, 257-274.
23. J. v. Tol, L.-C. Brunel and R. J. Wylde, *Rev. Sci. Instrum.*, 2005, **76**, 074101.
24. H. Blok, J. A. J. M. Disselhorst, S. B. Orlinskii and J. Schmidt, *J. Magn. Reson.*, 2004, **166**, 92-99.
25. T. A. Siaw, A. Leavesley, A. Lund, I. Kaminker and S. Han, *J. Magn. Reson.*, 2016, **264**, 131-153.
26. P. Neugebauer and A.-L. Barra, *Appl. Magn. Reson.*, 2010, **37**, 833-843.
27. P. Neugebauer, Ph.D., University of Grenoble, 2010.
28. S. S. Eaton, R. W. Quine, M. Tseitlin, D. G. Mitchell, G. A. Rinard and G. R. Eaton, in *Multifrequency Electron Paramagnetic Resonance*, Wiley-VCH, 2014, pp. 3-67.
29. J. S. Hyde, R. A. Strangeway, T. G. Camenisch, J. J. Ratke and W. Froncisz, *J. Magn. Reson.*, 2010, **205**, 93-101.
30. A. Doll, S. Pribitzer, R. Tschaggelar and G. Jeschke, *J. Magn. Reson.*, 2013, **230**, 27-39.
31. P. E. Spindler, Y. Zhang, B. Endeward, N. Gershernzon, T. E. Skinner, S. J. Glaser and T. F. Prisner, *J. Magn. Reson.*, 2012, **218**, 49-58.
32. P. E. Spindler, P. Schöps, W. Kallies, S. J. Glaser and T. F. Prisner, *J. Magn. Reson.*, 2017, **280**, 30-45.
33. K. Mobius, A. Savitsky, A. Schnegg, M. Plato and M. Fuchs, *Phys. Chem. Chem. Phys.*, 2005, **7**, 19-42.
34. J. A. Weil and J. R. Bolton, *Electron Paramagnetic Resonance: Elementary Theory and Practical Applications*, Wiley, 2nd edn., 2006.
35. J. Keeler, *Understanding NMR Spectroscopy*, 2nd edn., 2010.
36. V. L. Granatstein, R. K. Parker and C. M. Armstrong, *Proceedings of the IEEE*, 1999, **87**, 702-716.
37. P. M. Champion and A. J. Sievers, *J. Chem. Phys.*, 1980, **72**, 1569-1582.
38. P. L. Richards, *J. Appl. Phys.*, 1963, **34**, 1237-1238.
39. A. A. Mukhin, V. D. Travkin, A. K. Zvezdin, S. P. Lebedev, A. Caneschi and D. Gatteschi, *EPL (Europhysics Letters)*, 1998, **44**, 778.
40. A. Mukhin, B. Gorshunov, M. Dressel, C. Sangregorio and D. Gatteschi, *Phys. Rev. B*, 2001, **63**, 214411.

41. J. van Slageren, S. Vongtragool, B. Gorshunov, A. A. Mukhin, N. Karl, J. Krzystek, J. Telser, A. Muller, C. Sangregorio, D. Gatteschi and M. Dressel, *Phys. Chem. Chem. Phys.*, 2003, **5**, 3837-3843.
42. K. Ray, A. Begum, T. Weyhermüller, S. Piligkos, J. van Slageren, F. Neese and K. Wieghardt, *J. Am. Chem. Soc.*, 2005, **127**, 4403-4415.
43. A. Schnegg, J. Behrends, K. Lips, R. Bittl and K. Holldack, *Phys. Chem. Chem. Phys.*, 2009, **11**, 6820-6825.
44. A. Schweiger and G. Jeschke, *Principles of Pulse Electron Paramagnetic Resonance*, Oxford University Press, 2001.
45. C. Altenbach, S. L. Flitsch, H. G. Khorana and W. L. Hubbell, *Biochemistry*, 1989, **28**, 7806-7812.
46. W. L. Hubbell and C. Altenbach, *Current Opinion in Structural Biology*, 1994, **4**, 566-573.
47. T. F. Prisner, in *Biolog. Magn. Reson.*, 2004, vol. 22, pp. 249-272.
48. K. S. Novoselov, A. K. Geim, S. V. Morozov, D. Jiang, Y. Zhang, S. V. Dubonos, I. V. Grigorieva and A. A. Firsov, *Science*, 2004, **306**, 666-669.
49. P. R. Wallace, *Phys. Rev.*, 1947, **71**, 622-634.
50. M. Orlita, C. Faugeras, P. Plochocka, P. Neugebauer, G. Martinez, D. K. Maude, A. L. Barra, M. Sprinkle, C. Berger, W. A. de Heer and M. Potemski, *Phys. Rev. Lett.*, 2008, **101**, 267601.
51. A. K. Geim and K. S. Novoselov, *Nat Mater*, 2007, **6**, 183-191.
52. A. K. Geim, *Science*, 2009, **324**, 1530-1534.
53. C. Berger, Z. Song, X. Li, X. Wu, N. Brown, C. Naud, D. Mayou, T. Li, J. Hass, A. N. Marchenkov, E. H. Conrad, P. N. First and W. A. de Heer, *Science*, 2006, **312**, 1191-1196.
54. C. Berger, Z. Song, T. Li, X. Li, A. Y. Ogbazghi, R. Feng, Z. Dai, A. N. Marchenkov, E. H. Conrad, P. N. First and W. A. de Heer, *J. Phys. Chem. B*, 2004, **108**, 19912-19916.
55. J. K. Galt, W. A. Yager and H. W. Dail, *Physical Review*, 1956, **103**, 1586-1587.
56. P. Neugebauer, M. Orlita, C. Faugeras, A. L. Barra and M. Potemski, *Phys. Rev. Lett.*, 2009, **103**, 136403.
57. A. S. Mayorov, D. C. Elias, I. S. Mukhin, S. V. Morozov, L. A. Ponomarenko, K. S. Novoselov, A. K. Geim and R. V. Gorbachev, *Nano Letters*, 2012, **12**, 4629-4634.
58. M. Orlita, P. Neugebauer, C. Faugeras, A. L. Barra, M. Potemski, F. M. D. Pellegrino and D. M. Basko, *Phys. Rev. Lett.*, 2012, **108**, 017602.
59. R. E. Doezema, W. R. Datars, H. Schaber and A. Van Schyndel, *Phys. Rev. B*, 1979, **19**, 4224-4230.
60. D. Gatteschi, R. Sessoli and J. Villain, *Molecular Nanomagnets*, Oxford University Press, 2006.
61. A. Caneschi, D. Gatteschi, R. Sessoli, A. L. Barra, L. C. Brunel and M. Guillot, *J. Am. Chem. Soc.*, 1991, **113**, 5873-5874.
62. R. Sessoli, D. Gatteschi, A. Caneschi and M. A. Novak, *Nature*, 1993, **365**, 141.
63. J. R. Friedman, M. P. Sarachik, J. Tejada and R. Ziolo, *Phys. Rev. Lett.*, 1996, **76**, 3830-3833.
64. L. Thomas, F. Lionti, R. Ballou, D. Gatteschi, R. Sessoli and B. Barbara, *Nature*, 1996, **383**, 145.
65. L. Gregoli, C. Danieli, A.-L. Barra, P. Neugebauer, G. Pellegrino, G. Poneti, R. Sessoli and A. Cornia, *Chem. Eur. J.*, 2009, **15**, 6456-6467.
66. J. Tang and P. Zhang, *Lanthanide Single Molecule Magnets*, Springer-Verlag, Berlin Heidelberg, 2015.
67. T. Lis, *Acta Cryst. B*, 1980, **36**, 2042-2046.
68. R. Inglis, L. F. Jones, C. J. Milios, S. Datta, A. Collins, S. Parsons, W. Wernsdorfer, S. Hill, S. P. Perlepes, S. Piligkos and E. K. Brechin, *Dalton Trans.*, 2009, 3403-3412.

69. C. J. Milios, R. Inglis, A. Vinslava, R. Bagai, W. Wernsdorfer, S. Parsons, S. P. Perlepes, G. Christou and E. K. Brechin, *J. Am. Chem. Soc.*, 2007, **129**, 12505-12511.
70. O. Waldmann, *Inorg. Chem.*, 2007, **46**, 10035-10037.
71. F. Neese and D. A. Pantazis, *Faraday Discussions*, 2011, **148**, 229-238.
72. R. Layfield and M. Murugesu, *Lanthanides and Actinides in Molecular Magnetism*, Weinheim, Wiley-VCH edn., 2015.
73. S. T. Liddle and J. van Slageren, *Chemical Society Reviews*, 2015, **44**, 6655-6669.
74. C. A. P. Goodwin, F. Ortu, D. Reta, N. F. Chilton and D. P. Mills, *Nature*, 2017, **548**, 439.
75. J. Rozboril, Y. Rechkemmer, D. Bloos, F. Munz, C. N. Wang, P. Neugebauer, J. Cechal, J. Novak and J. van Slageren, *Dalton Trans.*, 2016, **45**, 7555-7558.
76. M. Mannini, F. Pineider, P. Sainctavit, C. Danieli, E. Otero, C. Sciancalepore, A. M. Talarico, M.-A. Arrio, A. Cornia, D. Gatteschi and R. Sessoli, *Nat. Mater.*, 2009, **8**, 194-197.
77. M. Mannini, F. Bertani, C. Tudisco, L. Malavolti, L. Poggini, K. Misztal, D. Menozzi, A. Motta, E. Otero, P. Ohresser, P. Sainctavit, G. G. Condorelli, E. Dalcanale and R. Sessoli, *Nat. Commun.*, 2014, **5**.
78. M. N. Leuenberger and D. Loss, *Nature*, 2001, **410**, 789-793.
79. M. N. Leuenberger and D. Loss, *Phys. Rev. B*, 2000, **61**, 12200-12203.
80. A. Ardavan, O. Rival, J. J. L. Morton, S. J. Blundell, A. M. Tyryshkin, G. A. Timco and R. E. P. Winpenny, *Phys. Rev. Lett.*, 2007, **98**, 057201.
81. L. Bogani and W. Wernsdorfer, *Nat Mater*, 2008, **7**, 179-186.
82. A. R. Rocha, V. M. García-suárez, S. W. Bailey, C. J. Lambert, J. Ferrer and S. Sanvito, *Nature Materials*, 2005, **4**, 335.
83. A. L. Barra, *Inorganica Chimica Acta*, 2008, **361**, 3564-3569.
84. L. Vergnani, A.-L. Barra, P. Neugebauer, M. J. Rodriguez-Douton, R. Sessoli, L. Sorace, W. Wernsdorfer and A. Cornia, *Chem. Eur. J.*, 2012, **18**, 3390-3398.
85. S. Petit, P. Neugebauer, G. Pilet, G. Chastanet, A.-L. Barra, A. B. Antunes, W. Wernsdorfer and D. Luneau, *Inorg. Chem.*, 2012, **51**, 6645-6654.
86. F. El Hallak, P. Neugebauer, A.-L. Barra, J. van Slageren, M. Dressel and A. Cornia, *J. Magn. Reson.*, 2012, **223**, 55-60.
87. T. K. Prasad, G. Poneti, L. Sorace, M. J. Rodriguez-Douton, A.-L. Barra, P. Neugebauer, L. Costantino, R. Sessoli and A. Cornia, *Dalton Trans.*, 2012, **41**, 8368-8378.
88. Y.-Y. Zhu, T.-T. Yin, S.-D. Jiang, A.-L. Barra, W. Wernsdorfer, P. Neugebauer, R. Marx, M. Dorfel, B.-W. Wang, Z.-Q. Wu, J. van Slageren and S. Gao, *Chem. Commun.*, 2014, **50**, 15090-15093.
89. C. Aronica, Y. Chumakov, E. Jeanneau, D. Luneau, P. Neugebauer, A.-L. Barra, B. Gillon, A. Goujon, A. Cousson, J. Tercero and E. Ruiz, *Chem. Eur. J.*, 2008, **14**, 9540-9548.
90. D. Schweinfurth, Y. Rechkemmer, S. Hohloch, N. Deibel, I. Peremykin, J. Fiedler, R. Marx, P. Neugebauer, J. van Slageren and B. Sarkar, *Chem. Eur. J.*, 2014, **20**, 3475 – 3486.
91. K. Bader, D. Dengler, S. Lenz, B. Endeward, S.-D. Jiang, P. Neugebauer and J. van Slageren, *Nat. Commun.*, 2014, **5**, 5304.
92. E. Moreno Pineda, N. F. Chilton, R. Marx, M. Dörfel, D. O. Sells, P. Neugebauer, S.-D. Jiang, D. Collison, J. van Slageren, E. J. L. McInnes and R. E. P. Winpenny, *Nat. Commun.*, 2014, **5**, 5243.
93. I. Nemec, R. Marx, R. Herchel, P. Neugebauer, J. van Slageren and Z. Trávníček, *Dalton Trans.*, 2015, **44**, 15014-15021.
94. Y. Rechkemmer, J. E. Fischer, R. Marx, M. Dörfel, P. Neugebauer, S. Horvath, M. Gysler, T. Brock-Nannestad, W. Frey, M. F. Reid and J. van Slageren, *J. Am. Chem. Soc.*, 2015, **137**, 13114-13120.

95. A. Abhervé, M. Palacios-Corella, J. M. Clemente-Juan, R. Marx, P. Neugebauer, J. van Slageren, M. Clemente-León and E. Coronado, *J. Mater. Chem. C*, 2015, **3**, 7936-7945.
96. M. van der Meer, Y. Rechkemmer, F. D. Breitgoff, R. Marx, P. Neugebauer, U. Frank, J. van Slageren and B. Sarkar, *Inorg. Chem.*, 2016, **55**, 11944-11953.
97. M. van der Meer, Y. Rechkemmer, U. Frank, F. D. Breitgoff, S. Hohloch, C.-Y. Su, P. Neugebauer, R. Marx, M. Dörfel, J. van Slageren and B. Sarkar, *Chem. Eur. J.*, 2016, **22**, 13884-13893.
98. S. Realista, A. J. Fitzpatrick, G. Santos, L. P. Ferreira, S. Barroso, L. C. J. Pereira, N. A. G. Bandeira, P. Neugebauer, J. Hruby, G. G. Morgan, J. van Slageren, M. J. Calhorda and P. N. Martinho, *Dalton Trans.*, 2016, **45**, 12301-12307.
99. M. van der Meer, Y. Rechkemmer, F. D. Breitgoff, S. Dechert, R. Marx, M. Dorfel, P. Neugebauer, J. van Slageren and B. Sarkar, *Dalton Trans.*, 2016, **45**, 8394-8403.
100. M. Gysler, F. El Hallak, L. Ungur, R. Marx, M. Hakl, P. Neugebauer, Y. Rechkemmer, Y. Lan, I. Sheikin, M. Orlita, C. E. Anson, A. K. Powell, R. Sessoli, L. F. Chibotaru and J. van Slageren, *Chem. Sci.*, 2016, **7**, 4347-4354.
101. Y. Rechkemmer, F. D. Breitgoff, M. van der Meer, M. Atanasov, M. Hakl, M. Orlita, P. Neugebauer, F. Neese, B. Sarkar and J. van Slageren, *Nat. Commun.*, 2016, **7**, 10467.
102. J.-J. Liu, S.-D. Jiang, P. Neugebauer, J. van Slageren, Y. Lan, W. Wernsdorfer, B.-W. Wang and S. Gao, *Inorg. Chem.*, 2017, **56**, 2417-2425.
103. M. G. Sommer, R. Marx, D. Schweinfurth, Y. Rechkemmer, P. Neugebauer, M. van der Meer, S. Hohloch, S. Demeshko, F. Meyer, J. van Slageren and B. Sarkar, *Inorg. Chem.*, 2017, **56**, 402-413.
104. I. Nemec, R. Herchel, M. Kern, P. Neugebauer, J. van Slageren and Z. Trávníček, *Materials*, 2017, **10**, 249.
105. P. Lutz, D. Aguilà, A. Mondal, D. Pinkowicz, R. Marx, P. Neugebauer, B. Fåk, J. Ollivier, R. Clérac and J. van Slageren, *Phys. Rev. B*, 2017, **96**, 094415.
106. A. Abragam and B. Bleany, *Electron Paramagnetic Resonance of Transition Ions*, Dover Publications, Inc., New York, 1986.
107. C. Sauvée, M. Rosay, G. Casano, F. Aussenac, R. T. Weber, O. Ouari and P. Tordo, *Angew. Chem., Int. Ed.*, 2013, **52**, 10858-10861.
108. C. Sauvée, G. Casano, S. Abel, A. Rockenbauer, D. Akhmetzyanov, H. Karoui, D. Siri, F. Aussenac, W. Maas, R. T. Weber, T. Prisner, M. Rosay, P. Tordo and O. Ouari, *Chem. Eur. J.*, 2016, **22**, 5598-5606.
109. P. Neugebauer, J. G. Krummenacker, V. P. Denysenkov, G. Parigi, C. Luchinat and T. F. Prisner, *Phys. Chem. Chem. Phys.*, 2012, **15**, 6049 - 6056.
110. P. Neugebauer, J. G. Krummenacker, V. P. Denysenkov, C. Helmling, C. Luchinat, G. Parigi and T. F. Prisner, *Phys. Chem. Chem. Phys.*, 2014, **16**, 18781-18787.
111. A. S. Lilly Thankamony, J. J. Wittmann, M. Kaushik and B. Corzilius, *Progress in Nuclear Magnetic Resonance Spectroscopy*, 2017, **102-103**, 120-195.
112. A. W. Overhauser, *Phys. Rev.*, 1953, **92**, 411-415.
113. T. R. Carver and C. P. Slichter, *Phys. Rev.*, 1953, **92**, 212-213.
114. T. Maly, G. T. Debelouchina, V. S. Bajaj, K. N. Hu, C. G. Joo, M. L. Mak-Jurkauskas, J. R. Sirigiri, P. C. A. van der Wel, J. Herzfeld, R. J. Temkin and R. G. Griffin, *J. Chem. Phys.*, 2008, **128**, 052211−052219.
115. J. H. Ardenkjær-Larsen, B. Fridlund, A. Gram, G. Hansson, L. Hansson, M. H. Lerche, R. Servin, M. Thaning and K. Golman, *Proceedings of the National Academy of Sciences of the United States of America*, 2003, **100**, 10158-10163.
116. C. Griesinger, M. Bennati, H. M. Vieth, C. Luchinat, G. Parigi, P. Höfer, F. Engelke, S. J. Glaser, V. Denysenkov and T. F. Prisner, *Progress in Nuclear Magnetic Resonance Spectroscopy*, 2012, **64**, 4-28.

117. I. Solomon, *Phys. Rev.*, 1955, **99**, 559-565.
118. K. H. Hausser, Stehlik, D., *Advances in Magnetic Resonance*, 1968, **3**, 79-139.
119. J. Wolber, F. Ellner, B. Fridlund, A. Gram, H. Jóhannesson, G. Hansson, L. H. Hansson, M. H. Lerche, S. Månsson, R. Servin, M. Thaning, K. Golman and J. H. Ardenkjær-Larsen, *Nuclear Instruments and Methods in Physics Research Section A: Accelerators, Spectrometers, Detectors and Associated Equipment*, 2004, **526**, 173-181.
120. M. Reese, D. Lennartz, T. Marquardsen, P. Höfer, A. Tavernier, P. Carl, T. Schippmann, M. Bennati, T. Carlomagno, F. Engelke and C. Griesinger, *Appl Magn Reson*, 2008, **34**, 301-311.
121. A. Krahn, P. Lottmann, T. Marquardsen, A. Tavernier, M.-T. Turke, M. Reese, A. Leonov, M. Bennati, P. Hoefer, F. Engelke and C. Griesinger, *Phys. Chem. Chem. Phys.*, 2010, **12**, 5830-5840.
122. V. P. Denysenkov, M. J. Prandolini, A. Krahn, M. Gafurov, B. Endeward and T. F. Prisner, *Appl Magn Reson*, 2008, **34**, 289-299.
123. R. E. Hoffman, *J. Magn. Reson.*, 2006, **178**, 237-247.
124. G. Liu, M. Levien, N. Karschin, G. Parigi, C. Luchinat and M. Bennati, *Nature Chemistry*, 2017, **9**, 676.
125. M. Tseitlin, A. Dhami, R. W. Quine, G. A. Rinard, S. S. Eaton and G. R. Eaton, *Appl. Magn. Reson.*, 2006, **30**, 651-656.
126. J. W. Stoner, D. Szymanski, S. S. Eaton, R. W. Quine, G. A. Rinard and G. R. Eaton, *J. Magn. Reson.*, 2004, **170**, 127-135.
127. N. Bloembergen, E. M. Purcell and R. V. Pound, *Phys. Rev.*, 1948, **73**, 679-712.
128. J. Dadok and R. F. Sprecher, *J. Magn. Reson.*, 1974, **13**, 243-248.
129. B. Král and A. Blatná, *Slaboproudý obzor*, 2016, **72**.
130. R. Beeler, D. Roux, G. Béné and R. Extermann, *Phys. Rev.*, 1956, **102**, 295-295.
131. http://www.ebyte.it/library/hist/NMR_Tesla_cs.html).

9 ABSTRACT

High Frequency Electron Spin Resonance (HFESR) is a magneto-optical method where microwave frequencies, typically 100s of GHz (meV range), are used for excitations. The HFESR method is a powerful tool to investigate samples ranging from biomolecules, over metal centers to magnetic materials. It delivers high g-value resolution and access to large zero-field splittings (ZFS). In materials science, it is also applied for measurements of modern solid state materials like graphene, topological insulators etc. In studies of coupled metallic centers with large ZFS (called molecular magnets or single-molecule magnets (SMMs)), HFESR is an essential tool providing detailed information about the magnetic properties of these materials. Furthermore, in the recent boom of NMR hyperpolarization, HFESR has an indisputable role in NMR signal enhancement. In this habilitation work the current development of HFESR and its application to solid state and molecular materials together with applications to NMR signal enhancement are discussed.